DESIGN OF Ni-METAL ORGANIC FRAMEWORK (Ni-MOF(74)) FOR EFFICIENT CO_2 ADSORPTION

A Thesis Submitted to
the Graduate School of Engineering and Sciences of
İzmir Institute of Technology
in Partial Fulfillment of the Requirements for the Degree of

MASTER OF SCIENCE

in Chemical Engineering

by
Hande GÜRSEL

June 2024
İZMİR

We approve the thesis of **Hande GÜRSEL**

Examining Committee Members:

Prof. Dr. Fehime ÇAKICIOĞLU ÖZKAN
Department of Chemical Engineering, İzmir Institute of Technology

Prof. Dr. Aslı Yüksel ÖZŞEN
Department of Chemical Engineering, İzmir Institute of Technology

Assist. Prof. Berrin İKİZLER
Department of Chemical Engineering, Ege University

27 June 2024

Prof. Dr. Fehime ÇAKICIOĞLU ÖZKAN
Supervisor, Department of Chemical Engineering,
İzmir Institute of Technology

Prof. Dr. Aysun SOFUOĞLU
Head of the Department of Chemical Engineering

Prof. Dr. Mehtap EANES
Dean of the Graduate School of Engineering and Sciences

ACKNOWLEDGEMENTS

I would like to express my sincere gratitude to my advisor Prof. Dr. Fehime ÇAKICIOĞLU ÖZKAN for her guidance, support, endless understanding, and encouragement during my MSc study. I would also like to thank Res. Assist. Dr. Gizem SAYGI for her support during my thesis.

I am also grateful to the members of my thesis committee, Prof. Dr. Aslı Yüksel ÖZŞEN and Assist. Prof. Berrin İKİZLER for their guidance and understanding.

On a personal note, I would like to thank my family for their endless love, encouragement, and support. Their belief in me has been a constant source of strength and motivation.

This thesis is dedicated to all those who believed in me and provided me with the necessary tools and support to achieve my goals.

ABSTRACT

DESIGN OF Ni-METAL ORGANIC FRAMEWORK (Ni-MOF(74)) FOR EFFICIENT CO_2 ADSORPTION

The urgency the address high CO_2 concentrations in the Earth's atmosphere increases each day prompting collaborative efforts between industry and the science community to develop various solutions. Among these, carbon capture utilization and storage (CCUS) technologies are proven to be integral. Rooted in CO_2 adsorption, carbon capture forms the cornerstone of CCUS technologies. Consequently, developing effective CO_2 capture materials and designing systems capable of integrating these materials into real-world practical applications play a crucial role. In this study, one of the most promising materials for future CO_2 capture technologies, Ni-MOF-74, is synthesized, characterized, and tested for CO_2 adsorption capacity. Following the synthesis process Ni-MOF-74 is immobilized on acrylonitrile fabric in order to achieve a flexible and versatile structure with high CO_2 capacity that can be integrated in various applications. The highest surface area and CO_2 adsorption capacity achieved by the synthesized Ni-MOF-74 powder are 180 m^2/g and 1.98 mmol/g, respectively. Synthesized Ni-MOF-74 powder was successfully immobilized on an acrylic fabric substrate through the drip casting method. The resulting composite showed a decrease in CO_2 adsorption capacity only by 8% which is promising for practical applications and a fair compromise considering that the flexible structure offers an opportunity to be utilized in a wide range of scenarios.

ÖZET

VERİMLİ CO_2 ADSORPSİYONU İÇİN Ni-METAL ORGANİK ÇERÇEVESİNİN (Ni-MOF(74)) TASARIMI

Dünya atmosferindeki yüksek CO_2 oranı ve sebep olduğu küresel etkilere karşı atılması gereken adımların aciliyeti her geçen gün artmakta ve bilim ile endüstri arasındaki iş birliği çabalarını gerekli kılmaktadır. Bu yolda geliştirilmekte olan en önemli teknolojilerden biri de karbon yakalama, kullanım ve depolama (CCUS) teknolojileridir. Temelinde CO_2 adsorpsiyonu yatan CCUS teknolojilerinin etkili bir şekilde kullanımı CO_2 yakalama kapasitesi yüksek materyallerin geliştirilmesi ve pratik uygulamalara uygun hale getirilmesini gerektirmektedir. Bu çalışmada, gelecekteki CO_2 yakalama teknolojileri için en umut verici malzemelerden biri olan Ni-MOF-74 sentezlenmiş, karakterize edilmiş ve CO_2 adsorpsiyon kapasitesi test edilmiştir. Sentez sürecini takiben, Ni-MOF-74 akrilik kumaş üzerine çeşitli uygulamalarda kullanılabilecek esnek bir yapı elde etmek amacı ile yüklenmiştir. Bu çalışmada sentezlenmiş olan Ni-MOF-74 ile elde edilen en yüksek yüzey alanı ve CO_2 adsorpsiyon kapasitesi sırası ile 180 m^2/g ve 1.98 mmol/g'dır. Sentezlenen Ni-MOF-74 akrilik kumaş üzerine damlatma döküm yöntemi kullanılarak başarı ile yüklenmiştir. Elde edilen bu esnek yapı, CO_2 adsorpsiyon kapasitesinde yalnızca %8'lik bir azalma göstermiştir. Bu oran, pratik uygulamalar için umut vadederken malzemenin esnek yapısı, geniş bir uygulama alanında kullanılma olanağı sunmaktadır.

TABLE OF CONTENTS

LIST OF FIGURES

Figure **Page**

Figure **Page**

LIST OF TABLES

Table **Page**

CHAPTER 1

INTRODUCTION

According to the United Nations Environment Programme's Emissions Gap Report released in 2023, Global emissions of greenhouse gases (GHG) have surged to an unprecedented level of 57.4 gigatons of CO_2 equivalent ($GtCO_2e$) (UNEP 2023). According to this report, the energy sector is responsible for the largest part of these emissions with 36%, and is followed by the industry as the second largest contributor with 25% which are both heavily reliant on fossil fuels. Thus, it is clear that reducing emissions from these sectors is pivotal in the fight against global warming. Reducing this reliability on fossil fuels by fuel switching and incorporating renewable energy options into the infrastructure are the main actions that need to be taken to reduce emissions from these sectors. However, it is evident that the use of fossil fuels cannot be entirely cut off (Keskin, van Heest, and Sholl 2010a). This is why novel technologies must be developed to limit environmental destruction caused by the utilization of fossil fuels. As part of this effort, carbon capture utilization and storage (CCUS) technologies are viewed as an alternative strategy. CCUS is an innovative approach to the CO_2 problem involving the capture and separation of CO_2 from a point source or directly from the atmosphere followed by a utilization process or sequestration in geological structures (Greig and Uden 2021). The latest reports providing insights into climate mitigation state that CCUS technologies are an integral part of climate mitigation, especially in the power sector (Energy Agency, n.d.). IPCC AR6 states that global pathways modeled to limit warming below 2°C involve the application of energy generation technologies with CCUS (Calvin et al. 2023). Any CCUS technology starts with CO_2 capture through different approaches.

Currently, there are 5 different approaches to CO_2 capture technologies including post-combustion, pre-combustion, oxy-combustion, chemical looping combustion (CLC), and direct air capture (DAC) (Akpasi and Isa 2022; Olabi et al. 2022; X. Wang and Song 2020; Leung, Caramanna, and Maroto-Valer 2014; Sreenivasulu et al. 2015).

CO_2 separation methods hold a crucial role in these approaches, especially in pre-combustion, post-combustion, and direct air capture approaches.

For CO_2 separation, 4 major techniques are utilized including absorption, adsorption, membrane separation, and cryogenic separation (Akpasi and Isa 2022; Olabi et al. 2022; X. Wang and Song 2020). Among these techniques, adsorption has attracted attention due to high processing capacity at ambient conditions, less energy-intensive regeneration process, high CO_2 capture potential, and improved selectivity (Yangyang Liu, Zhiyong U. Wang, and Hong-Cai Zhou 2012; Wilberforce et al. 2021). The adsorption process involves the use of solid materials for CO_2 capture. Physical or chemical interactions formed on the surface of these solid adsorbers are the driving force behind the absorption process (Sifat and Haseli 2019). Examples of adsorbents considered for CO_2 separation technologies include zeolites, metal-organic frameworks (MOFs), and calcium oxides. (Nakao Shin-ichiand Yogo 2019).

Among these adsorbents, MOFs have recently attracted great attention due to their promising properties. These solid-state materials are formed by controlled coordination of metal cations and organic ligands. This coordination leads to a porous crystalline structure with unique properties such as highly adjustable physical properties, high surface area and adsorption capacities, renderability, and affinity towards CO_2 (Hu et al. 2019; Ghanbari, Abnisa, and Wan Daud 2020; Liang et al. 2019; Fajrina et al. 2022; Pettinari and Tombesi 2020; Lin et al. 2023). Even though powder-form MOFs exhibit impressive qualities in laboratory environments, the practical application of MOFs requires the development of composite structures on supporting substrates (Ma et al. 2020; Teo et al. 2021; Choi et al. 2020). For this purpose, fibers and fabrics are considered suitable options due to their accessibility and low cost (Ma et al. 2020).

Even though there are a number of studies focusing on the synthesis and immobilization of MOFs onto fabric structures, there still exists a great need for further investigation into the assessment of CO_2 capture capacities of different MOFs, the immobilization process onto fabric structures, and the effect of immobilization on the CO_2 capture capacity. The objective of this study was to synthesize Ni-MOF-74, a highly promising MOF for CO_2 capture, immobilize the MOF structure onto acrylic fabrics and fibers, and assess the CO_2 capture capacity of both powder-form and MOF/fiber complex structures.

CHAPTER 2

METAL ORGANIC FRAMEWORKS (MOFS)

As the interest in improved applications for gas separation, gas storage, heterogenous catalysis, drug delivery, and storage increased, the value of porous materials has been acknowledged more and more. Within this arena, different organic materials such as activated carbon and inorganic structures such as zeolites have initially been explored. Considering the attractive properties of these organic and inorganic structures such as stability, high surface areas, and high adsorption capacities, it was intriguing to combine organic and inorganic materials (Kuppler et al. 2009). The resulting hybrid structure is widely known as metal organic frameworks (MOFs); however, it can also be cited as porous coordination networks, porous coordination polymers, or hybrid organic-inorganic materials (Kuppler et al. 2009; Kitagawa and Matsuda 2007; Yu et al. 2023).

2.1. Structure and Properties of MOFs

MOFs are well-defined crystalline structures comprised of metal ions and organic ligands. Metals in the structure act as connectors while organic ligands act as linkers to create a stable structure called secondary building units (SBUs). For the formation of these stable structures utilization of charged organic linkers and metal nodes are essential. This combination leads to the formation of a multinuclear structure with strong directional bonds (Kalmutzki, Hanikel, and Yaghi 2018). The frameworks of MOFs are formed by the connection of these SBUs (Kalmutzki, Hanikel, and Yaghi 2018; Rowsell and Yaghi 2004). Thanks to the predictable geometry and connectivity of these building units, the overall framework structure of the synthesized MOFs can be controlled which gives a unique distinction over other solid materials. It is possible to achieve various

geometrical structures and even combine SBUs with different geometries to tailor the framework of MOFs.

The pore size of MOFs can be modified by changing the length of the organic linker without affecting the overall geometry of the network or through different combinations of various SBU geometries. This unique property allows remarkable control over the targeted applications (Kalmutzki, Hanikel, and Yaghi 2018). Thanks to the porous structure, MOFs show high surface areas providing a wide range of advantages.

The functionality of MOFs can also be controlled by manipulating the organic linker molecules (Rowsell and Yaghi 2004) or utilizing different metal node configurations. The inclusion of chiral or active compounds within the MOF structure can functionalize the overall material (Safaei et al. 2019). These tailorable qualities rightly so attract great attention to MOFs.

Thanks to these desirable qualities, MOFs show great potential in gas storage, separation, adsorption, catalysis, and ion exchange (Hu et al. 2019; Fajrina et al. 2022; Pettinari and Tombesi 2020).

2.2. Synthesis of MOFs

Various synthesis options developed within the materials chemistry have been put to the test for MOF synthesis as well. These synthesis methods include solvothermal, microwave-assisted synthesis, mechanochemical, sonochemical, and electrochemical synthesis. Among these options, the solvothermal method is one of the most well-known synthesis options and is the most utilized method for MOF synthesis (Ghanbari, Abnisa, and Wan Daud 2020). This approach utilizes thermal energy for the reaction by heating the reagents (metal A mix of different solvents can also be utilized in order to adjust the properties of reaction media. The solvothermal synthesis method provides easier control over the properties and structure of MOFs by controlling the solvent properties, reaction time, and temperature (Rowsell and Yaghi 2004). The reaction time can vary between 1 hour to 6 days while the reaction temperature usually ranges between 350-473 K (Aniruddha, Sreedhar, and Reddy 2020).

As an alternative approach microwave-assisted synthesis has also been explored (Wu et al. 2013; C. Chen et al. 2019; Cho et al. 2012). This method involves the utilization of microwave irradiation to promote the synthesis reaction. Even though it is not applied as widely as the solvothermal synthesis method, it is found to be advantageous due to shortened reaction times (Safaei et al. 2019; Aniruddha, Sreedhar, and Reddy 2020).

Similar to microwave-assisted synthesis methods, the sonochemical method utilizes ultrasonic waves. High-energy ultrasound is found to be useful in increasing the temperature quickly and reducing the reaction time (Ghanbari, Abnisa, and Wan Daud 2020). In 2009, HKUST-1 was the first MOF synthesized by sonochemical method (Li et al. 2009). While reduced reaction time can be beneficial, it can also make it challenging to manipulate MOF properties through these synthesis methods in comparison to the solvothermal approach.

As another alternative synthesis method, electricity can be employed. Metal ions and dissolved organic linker along with an anode, cathode, and electrolyte solution for this synthesis method. This method also attracts attention due to shorter reaction times. However, this method might lead to decreased pore size and have an adverse effect on the crystal structure (Ghanbari, Abnisa, and Wan Daud 2020; Aniruddha, Sreedhar, and Reddy 2020).

The mechanochemical synthesis method differentiates from all of the above-mentioned methods because it does not necessitate the use of a solvent medium. In this method, MOFs are synthesized through mechanical forces such as grinding and tight mixing. Because there is no use of solvent in this method, it is considered to be more environmentally friendly (Safaei et al. 2019; Ghanbari, Abnisa, and Wan Daud 2020).

2.3. MOFs in CO_2 Capture

2.3.1. Interaction of CO_2 with MOFs

Thanks to the attractive properties of MOFs mentioned above, these nanoengineered materials are considered as one of the suitable materials for gas adsorption and

consequently CO_2 capture technologies. Exploring the possibility of harvesting MOFs power in gas adsorption has attracted many researchers who are focusing on CO_2 emission reduction technologies. In order to utilize the full potential of MOFs in this area, it is important to understand the general concepts behind adsorption through MOFs.

CO_2 adsorption in MOFs is predominantly governed by the interactions between the SBU structures and CO_2 molecules. Similar to other adsorbates such as zeolites, physisorption of CO_2 is observed on MOF surfaces. However, MOFs offer various additional functionalities for the increase of CO_2 uptake capacities. The fundamental functionalities offered by the MOF structure include open metal sites (OMSs) and Lewis basic sites (LBSs).

Utilization of OMSs is the most commonly used technique for increasing the adsorption capacity of MOFs. This strategy is based on harvesting the interaction between CO_2 molecules and unsaturated metal nodes which act as Lewis acid (Kalmutzki, Hanikel, and Yaghi 2018). This is why, OMSs are sometimes also called Lewis acid sites (LASs) (Ding et al. 2019). In order to decorate MOF structure with OMSs, solvent molecules that interacted with the metal nodes during the synthesis process are removed through thermal treatment usually under vacuum. Removal of these solvent molecules leaves the metal nodes unsaturated and ready for interaction with CO_2 molecules (Choe, Kim, and Hong 2021; Ding et al. 2019). However, it is important to note that, even though OMSs strongly increase the CO2 adsorption capacity, these polar sites also show affinity to H2O molecules which creates a competitive adsorption environment. This is why, a decrease in CO2 adsorption capacity may be observed under humid conditions (Kalmutzki, Hanikel, and Yaghi 2018; Choe, Kim, and Hong 2021). The effect of OMSs not only improves the CO_2 capture capacity of MOFs but also imparts a selective adsorption property for gas separation. The polar nature of these unsaturated metal sites shows a greater affinity towards polarizable molecules. For example, a higher affinity towards CO_2 over H_2 molecules leads to effective CO_2/H_2 separation (Ding et al. 2019).

Another strategy employed for enhancing the CO_2 capture capacity of MOFs is to incorporate organic linkers containing Lewis basic sites (LBSs). In this case, CO_2 acts as Lewis acid against the Lewis basic properties of the organic linker. Most commonly, organic ligands containing, or conditioned to contain, amine groups are explored for imparting these LBSs to MOF structure. This approach is based on the excellent CO_2 capture capacity of traditional absorbent monoethanolamine (MEA). The chemical absorption behavior of CO_2 can be replicated in the MOF structure through the utilization

of amine groups (Ghanbari, Abnisa, and Wan Daud 2020; Ding et al. 2019). Even though amine-based linkers are the most commonly studied option for LBSs, other nitrogenous groups such as $C_4H_4N_2$, $C_3H_3N_3$, and $C_5H_5N_5$ (Ding et al. 2019; Nandi et al. 2021). Lewis acid-base interactions between CO_2 and linkers lead to a reduced effect of H_2O on the CO_2 capture capacities of MOFs which can be beneficial for applications under humid conditions. However, it is important to note that, chemisorptive behavior between CO_2 and linkers may affect the regeneration capabilities of the synthesized MOFs. Furthermore, the inclusion of nitrogenous groups may lead to an overdecorated pore vicinity and hinder physical access of CO_2 into the MOF structure. Hence, careful design of LBSs is crucial (Ghanbari, Abnisa, and Wan Daud 2020; Ding et al. 2019).

Carboxylate or hydroxide groups can also be utilized to improve the CO_2 capacity of MOFs. While carboxylate groups reduce the effect of humidity due to the polar properties hydroxide groups strengthen the immediate interaction between the metal node and the CO_2 molecules (Pettinari and Tombesi 2020).

Another property to pay attention to when it comes to the selective adsorption of CO_2 molecules is the pore size. Considering the kinetic diameter of CO_2 (3.3 Å), the MOF structure can be tailored to target selective CO_2 adsorption (Q. Wang et al. 2016).

2.3.2. Potential MOFs for CO_2 Capture

In order to utilize the promising CO_2 capture potential of these hybrid frameworks, a range of MOFs have been investigated by different researchers. These studies aim to determine the CO_2 adsorption capacities of different MOFs under a wide array of conditions, including varying temperatures and pressures. Table 1 below provides a list of the most commonly studied MOFs for CO_2 capture, summarizing the performance metrics under different testing conditions. This compilation serves a valuable resource for understanding the variable CO_2 adsorption capacities of these novel materials. This table also demonstrates that the same MOF may show a range of CO_2 adsorption capacities rather than a fixed characteristic value.

Table 1. CO_2 adsorption capacities of commonly studied MOFs

MOF	**CO_2 Adsorption Capacity (mmol/g)**	**Temperature - Pressure (K – bar)**	**Reference**
Ni-MOF-74	0.38-6.68	298 - 1	(Rezaei et al. 2017a; Choe, Kim, and Hong 2021; D. L. Chen et al. 2014)
Mg-MOF-74	9	298 - 1	(Choe, Kim, and Hong 2021)
Co-MOF-74	6.9	298 - 1	(Choe, Kim, and Hong 2021)
HKUST-1	1.8-5	298 - 1	(Keskin, van Heest, and Sholl 2010b; Yazaydın et al. 2009)
MOF-177	33.5	298 - 35	(Millward and Yaghi 2005)
UiO-66	2.3-3	273 - 1	(Pettinari and Tombesi 2020; Ding et al. 2019)
UTSA-16	3.7	298 - 1	(Rezaei et al. 2017a)
ZIF-8	2.7	298 - 1	(Yazaydin et al. 2009)
MOF-200	54.5 mmol/g	298 - 50	(Pettinari and Tombesi 2020)

Within the scope of this work, only OMSs-based MOFs have been considered amongst the most commonly studied MOF structures in the literature. As the table suggests, MOF-74 type adsorbents offer high CO_2 capture capacities. In fact, the CO_2 capture capacities of these isoreticular structures are quite similar and show changes within a similar range (Choe, Kim, and Hong 2021; Ding et al. 2019; Pettinari and Tombesi 2020; Keskin, van Heest, and Sholl 2010b). Having said that, Mg-MOF-74 stands out as it generally shows the highest CO_2 adsorption capacity. Following that Ni-MOF-74 attracts attention since it is reported as the most stable MOF-74 variant in the presence of water (Liu et al. 2011).

Based on the information provided above, Ni-MOF-74 is found to be a suitable option for CO_2 capture studies. To this date, various studies focusing on the CO_2 capture

properties of Ni-MOF-74 have been conducted. According to these studies, the CO_2 capture capacity of Ni-MOF-74 is based on the effect of OMSs (Pettinari and Tombesi 2020), Ni-MOF-74 shows good thermal stability, and a highly porous nature (C. Chen et al. 2019). A wide range of results concerning the surface area of Ni-MOF-74 has been reported. BET surface area of Ni-MOF-74 samples ranged between 599 m^2/g (Grant Glover et al. 2011) and 3,398 m^2/g (Rezaei et al. 2017a). Similarly, the reported CO_2 capture capacities of Ni-MOF-74 range between 0.38 mmol/g (Kamal et al. 2020) and 6.68 mmol/g (C. Chen et al. 2019).

Table 2. CO_2 adsorption potential of Ni-MOF-74

MOF	**CO_2 Adsorption Capacity (mmol/g)**	**Temperature - Pressure (K – bar)**	**Synthesis Method**	**Reference**
Ni-MOF-74	0.38	298 - 1	Solvothermal	(Kamal et al. 2020)
	5.8	298 - 1	Solvothermal	(Kamal et al. 2020)
	2.5	298 - 1	Solvothermal	(Chen et al. 2014)
	5.64/4.54	273/298 - 1	Solvothermal	(C. Chen et al. 2019)
	6.68/5.5	273/298 - 1	Microwave assisted	(C. Chen et al. 2019)
	6.54	298 - 1	Solvothermal	(Rezaei et al. 2017b)

2.4. Immobilization of Ni-MOF-74

Despite their significant potential in various technologies such as CO_2 capture, practical integration of MOFs into existing requires integration into carriers. For this purpose, immobilization of Ni-MOF-74 has been studied as well. Such studies include the immobilization of Ni-MOF-74 onto monoliths (Rezaei et al. 2017a), metal plates, metal foams, metal gauzes (Jodłowski et al. 2020), carbon fibers (Martinez-Diaz et al. 2024), and PAN fibers (Harandizadeh et al. 2022; Amini et al. 2020). Even though the reported studies on Ni-MOF-74 integration into different carrier structures are targeted to various applications, the common purpose of these studies remains the same: easy integration of MOFs into real-world applications. However, the immobilization of Ni-

MOF-74 on woven fabrics, which are flexible, multipurpose, and one of the most affordable supporting structures, has not been explored yet.

For MOF immobilization, various techniques have been reported including *in situ* methods such as direct solvothermal deposition, layer-by-layer growth, and inkjet printing methods; and *ex situ* methods such as electrospinning and dip coating (Ma et al. 2020; Rezaei et al. 2017a). For direct solvothermal deposition method involves including the supporting material directly into the synthesis solution. The MOF particles are deposited on the supporting material during the synthesis process. However, this method might not provide a controlled deposition onto the surface since nucleation occurs within the reaction solvent rather than the support surface (Ma et al. 2020). Layer-by-layer growth involves subsequent immersion of the supporting substrate into metal salt and organic linker solutions. This leads to a gradual growth of MOF layers on the substrate surface. This technique offers a controlled synthesis of MOFs on the supporting structure (Rezaei et al. 2017a). The inkjet printing method emerges as a novel immobilization technique, and it is based on the evaporation-induced crystallization technique. The synthesis solution combined with stabilizing agents is loaded into a printing mechanism and printed onto the supporting substrate (Goel et al. 2021). This method offers the flexibility of controlling the MOF loading shape and thickness. The electrospinning method is one of the most commonly utilized *ex situ* deposition methods for MOFs. The electrospinning method involves mixing readily synthesized MOF particles into a polymer medium to create a suspension. This suspension is then subjected to high voltage to create thin fibers (Harandizadeh et al. 2022; Amini et al. 2020). The electrospinning technique compliments the high surface area of MOFs. The dip coating method is a commonly used coating method, especially in the textile industry. This method can also be adjusted for immobilization of MOFs. For the dip coating technique, the supporting substrate is dipped into an MOF/polymer mixture. The thickness of the MOF layer can be controlled during the dipping steps (Ma et al. 2020). These methods have all been considered for the immobilization of Ni-MOF-74 onto different supporting surfaces.

CHAPTER 3

CO_2 ADSORPTION

Adsorption is a fundamental process that involves the attraction of molecules, ions, or atoms from a gas bulk face to the surface of a solid phase due to intermolecular forces, coulomb forces, or electron transfer. Within the adsorption system, molecules of the gas phase are called the “adsorbate” while the solid surface is called the “adsorbent” (Bastos-Neto, de Azevedo, and de Lucena 2020). During the adsorption process, gas or liquid particles adhere to the surface of the adsorbent resulting in an exothermic interaction. Removal of these gas or liquid particles from the adsorbent surface is denoted as desorption which is an endothermic process as opposed to adsorption.

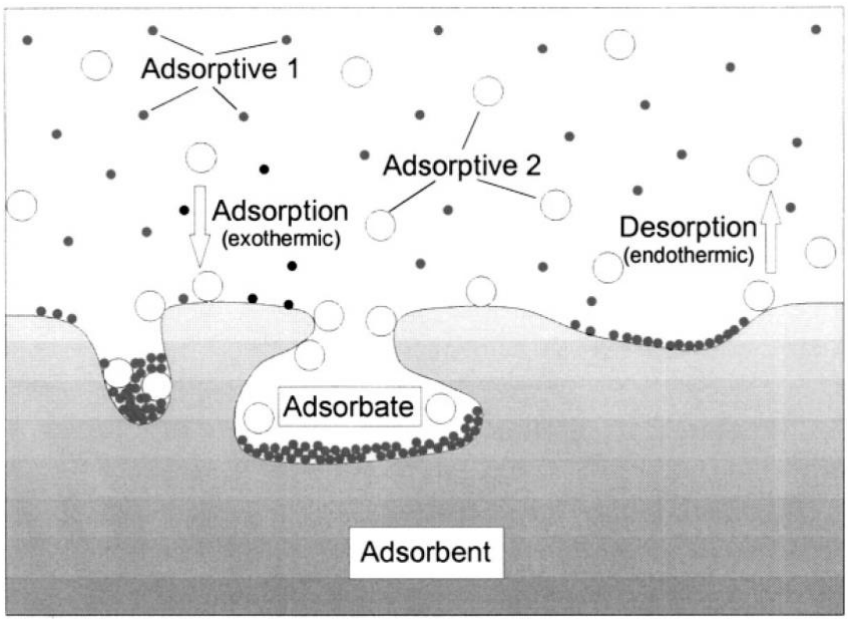

Figure 1. Adsorption process (Source: Jürgen U. Keller and Reiner Staudt 2005)

Based on the nature of attractive forces between the adsorbent and adsorbate, adsorption can be classified as physisorption or chemisorption. In physisorption, physical forces such as van der Waals forces and Coulomb forces are in effect. Coulomb forces are predominantly observed in the case of charged adsorbates while van der Waals interactions are predominately observed in the case of neutral adsorbates. On the other hand, chemisorption involves electron transfer between the adsorbate and adsorbent leading to a stronger interaction (Ruthven 2001). Due to the stronger interaction and electron transfer between adsorbate and adsorbent, the nature of chemisorption can be described as irreversible. The need for electron transfer between the adsorbate and adsorbent surface also means that the adsorption is observed in a monolayer at the adsorbent surface. On the other hand, physical adsorption can be observed in multilayers.

3.1. Adsorption Isotherms

Considering that adsorption is governed by thermodynamic rules, the first phenomenon related to adsorption is to be taken as Henry's law. Following Henry's law, an adsorption isotherm dependent on the adsorbed adsorbate amount and partial pressure of the system can be expressed. Henry's adsorption isotherm deals with low surface coverage concentrations.

$$q = K'P \tag{3.1}$$

As can be observed from the structure of this equation, Henry's adsorption isotherm follows a linear form. The slope of this linear adsorption isotherm is known as Henry's law constant (K'). The temperature dependence of Henry's constant, acting as a thermodynamic equilibrium constant, adheres to the basic van't Hoff equation (Ruthven 2001):

$$\lim_{p \to 0} \left(\frac{dq}{dp} \right) = K' = K'_0 e^{-\Delta H_0 / RT} \tag{3.2}$$

As the surface coverage concentrations increase the isotherm diverges from ideal linear form and becomes more complex. Such isotherms can be categorized as summarized in Figure 2.

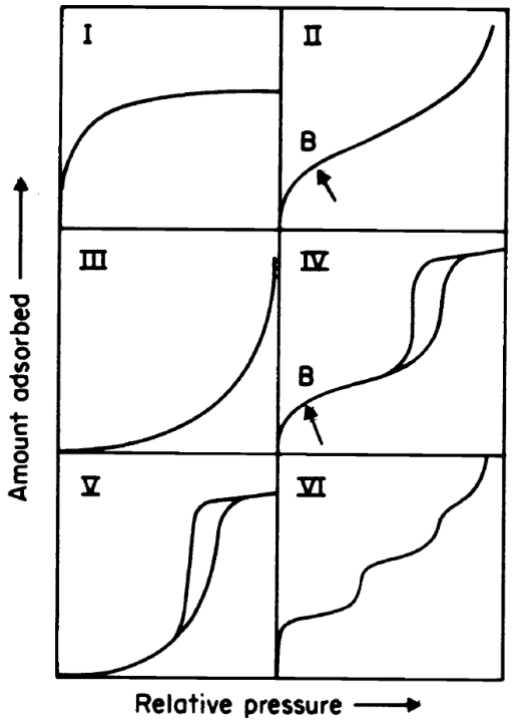

Figure 2. Classification of adsorption isotherms (Source: IUPAC 1985)

In order to have a deeper understanding of the adsorption interactions between the liquid phase and solid surface, various other isotherm models have been developed over the history of science. These isotherms are not only utilized for understanding the adsorptive behavior but also an integral device for the characterization of porous solids. Depending on the specific adsorption system, different isotherm models can be considered.

Amongst the various adsorption models, the Langmuir model provides one of the most commonly referred equilibria of adsorptions and is found to be useful for understanding monolayer adsorption. Langmuir adsorption isotherm follows certain assumptions that are outlined as follows (Douglas M. Ruthven 1984).

1. Clearly defined and a fixed number of adsorption sites are available on the surface,
2. Each active site can interact with one adsorbate molecule,
3. All active sites are energetically equivalent, and
4. Gas molecules behave ideally meaning that adsorbed molecules do not interact with each other.

$$\frac{q}{q_s} = \frac{bp}{1 + bp} \tag{3.3}$$

In this equation, q represents the adsorbed amount, q_s represents saturation limit, b is the equilibrium constant, and p represents pressure. For the Langmuir model, the equilibrium constant can be expressed in terms of Henry's constant with the following equilibrium.

$$b = K'q_s \tag{3.4}$$

Consequently, the Langmuir equilibrium of adsorption approaches Henry's Law at low pressures (Ruthven 2001).

Another adsorption model that is commonly referred to is the Freundlich adsorption model. This model is found to be useful in expressing the multilayer adsorption behavior on heterogenous surfaces. Freundlich adsorption isotherm follows the equation below.

$$q = bp^{1/n} \tag{3.5}$$

In this equation n is the equilibrium parameter which represents the heterogeneity of the system (Lesmana et al. 2009). Freundlich adsorption model assumes that the adsorbent surface presents heterogenous active adsorption sites with different adsorption energy.

CHAPTER 4

EXPERIMENTAL STUDIES

4.1. Materials

Acrylic fibers were sourced readily made. Two different acrylic fabric samples were used for immobilization experiments. One of the samples represent standard acrylic fabric (AK700) while the other represents an acrylic fabric produced for outdoor usage with smooth surface (ATIII). Materials used in the synthesis and immobilization of Ni-MOF-74 are listed in Table 3 below. No further purification was applied.

Table 3. Materials used for experimental studies

Material	Chemical Formula
Nickel(II) nitrate hexahydrate	$Ni(NO_3)_2.6H_2O$
2,5-dihydroxyterephthalic acid (DHTA)	$C_8H_6O_6$
N, N- dimethylformamide (DMF)	$HCON(CH_3)_2$
Methanol	CH3OH
Ethanol	C_2H_6O
Polyacrylic acid (PAA)	$(C3H_4O_2)_n$

4.2. Synthesis of Ni-MOF-74

The Ni-MOF-74 was synthesized in accordance with previously published solvothermal procedures (Wu et al. 2013; Haque and Jhung 2011) with several

adjustments. In order to understand the effect of molar ratios on Ni-MOF-74 properties, different molar ratios between nickel salt and organic ligand were applied (1:1 and 2:1 ratios).

First, 0.369 g of 2,5-Dihydroxyterephthalic Acid and 0.582 g of Nickel(II) nitrate hexahydrate (1:1 molar ratio) were dissolved in a mixture of 80 mL DMF and 5 mL distilled water (DW) in equimolar quantities under stirring at room temperature. Throughout the thesis, this sample is denoted as MOF-74(1:1). Resulting solution in a sealed heat-resistant glass flask (500 ml) was then placed in a sonic bath at 70°C for 1 hour in order to achieve a homogenous solution. This solution was then placed in an oven (Binder ED 53 and Memmert 100-800) at a crystallization temperature of 110 °C for 24 hours. The crystallization reaction resulted in brown particles collected at the bottom of the flask. Before separating the MOF particles from the mother liquor, the solution was left to cool down to room temperature for 2 hours. Ni-MOF-74 particles were then separated from the mother liquor by filtration. After this separation step, Ni-MOF-74 crystals were washed with absolute methanol twice. Washed crystals were left in a desiccator for 3 days to dry out before they were dried further in a vacuum drying oven at 150°C for 7 hours. MOF-74(1:1) synthesis procedure is demonstrated in Figure 3 below.

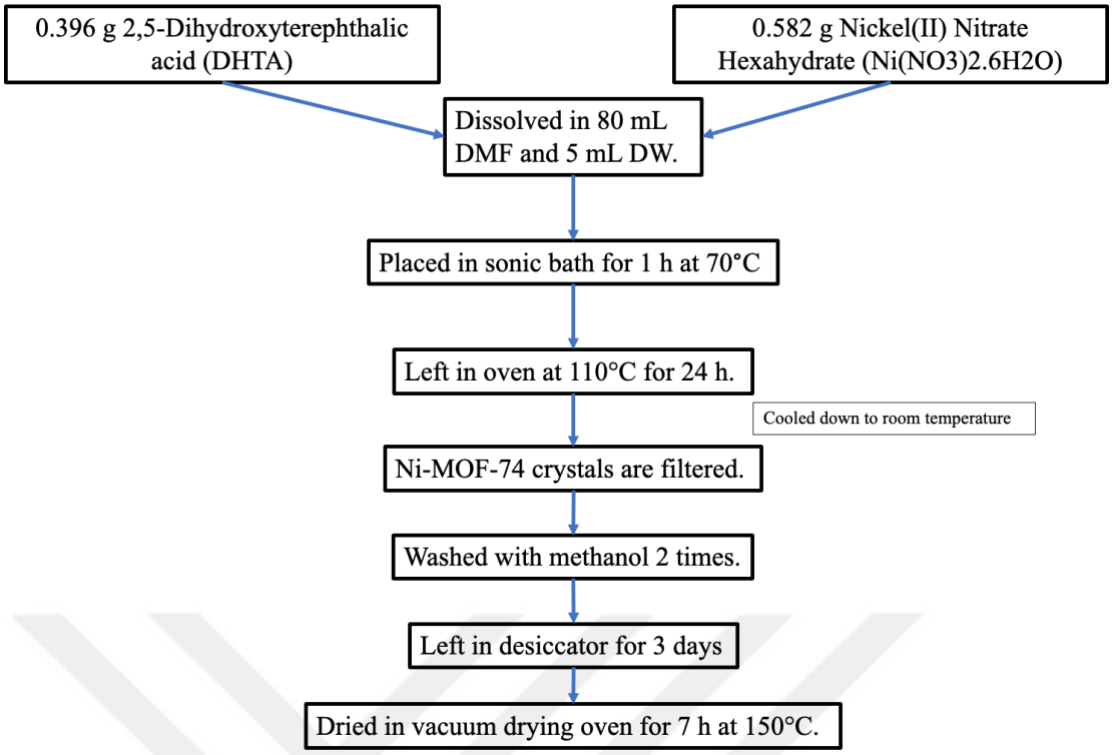

Figure 3. Synthesis procedure for MOF-74(1:1)

For the Ni-MOF-74 sample with a 2:1 molar ratio, the same synthesis procedure is applied. However, 0.369 g of 2,5-Dihydroxyterephthalic Acid and 1.164 g of Nickel(II) nitrate hexahydrate (2:1 molar ratio) were dissolved in a mixture of 80 mL DMF and 5 mL distilled water (DW) under stirring at room temperature. Throughout the thesis, this sample is denoted as MOF-74(2:1). The MOF-74(2:1) synthesis procedure is demonstrated in Figure 4 below.

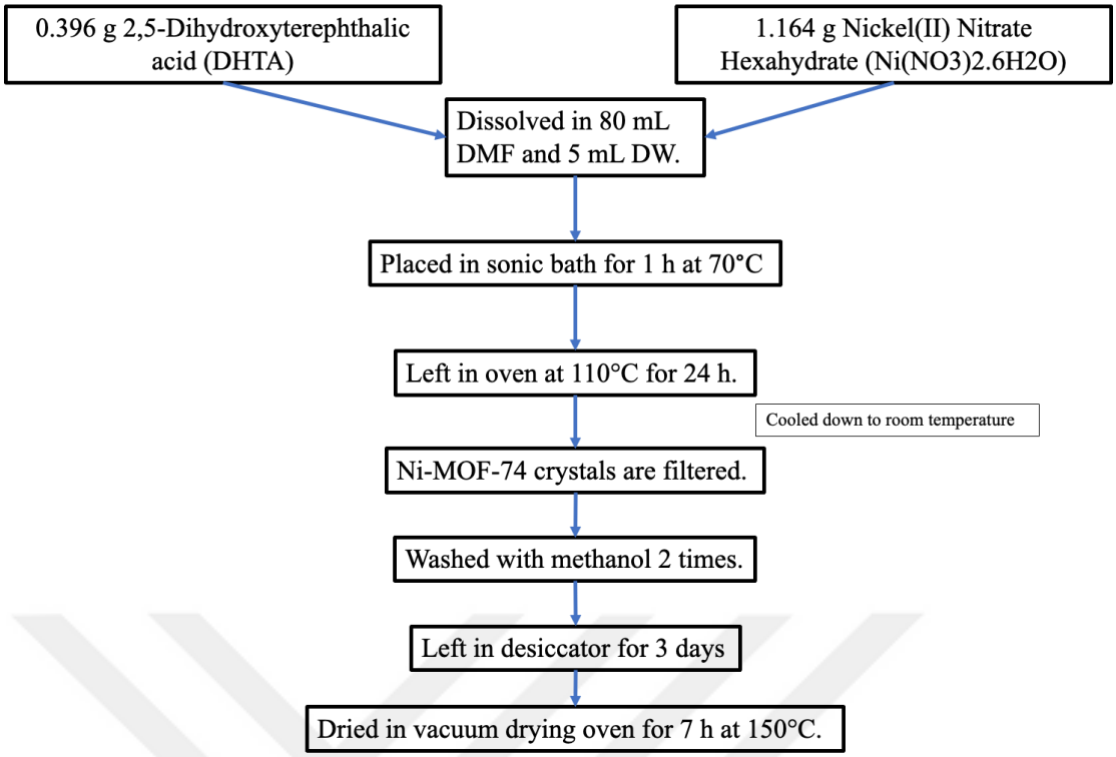

Figure 4. Synthesis procedure for MOF-74(2:1)

4.3. Immobilization of Ni-MOF-74 on Acrylic Fabrics

The immobilization experiments were only carried out for MOF-74(1:1) because this sample presented a higher CO_2 adsorption capacity. Experiments were carried out following two different techniques, *in-situ* dip coating (Rezaei et al. 2017a) and drip casting (Teo et al. 2021). All techniques were applied the same for both fabric types (AK700 and ATIII)

For the *in-situ* dip coating method, a previously published technique utilized for immobilization of Ni-MOF-74 on monolithic structures was adopted (Rezaei et al. 2017a). The exact Ni-MOF-74 synthesis method was followed up to the sonification step as mapped out in Section 4.2 above. After the sonication step, acrylic fabric pieces cut to 2 cm x 2 cm size were added to the synthesis mixture. After the addition of fabric pieces to the mother liquor, the same synthesis steps were followed as well. The *in-situ* dip coating procedure is demonstrated in Figure 5 below.

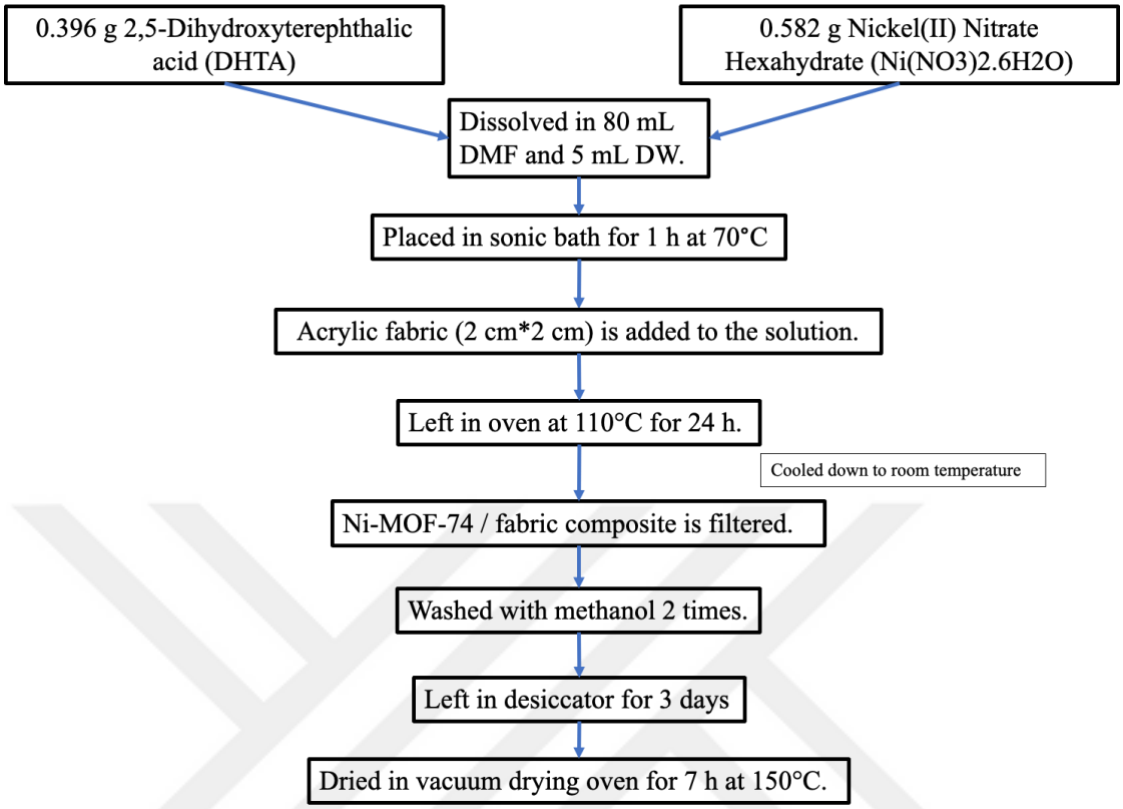

Figure 5. Procedure for *in-situ* Dip Coating Method

For the drip casting method, immobilization of readily synthesized Ni-MOF-74 particles was carried out by adopting a previously published technique applied for different MOFs (HKUST-1, MIL-101(Cr), MIL-100(Fe), and UiO-66) and fabrics (Teo et al. 2021).

Before the immobilization step, acrylic fabrics (2 cm x 2 cm) were soaked in absolute ethanol and dried in the oven. First, Ni-MOF-74 crystals on acrylic fabrics, an MOF-ink was obtained by mixing readily synthesized Ni-MOF-74 particles (0.03 g) and Poly(acrylic) acid (PAA) (0.03 g) in the presence of 0.5 mL absolute ethanol. The resulting viscous MOF-ink was then dripped on acrylic fiber pieces. As the last step, this MOF-ink/acrylic fabric composite was dried in the oven at 60°C for 1 hour and stored in a desiccator. The immobilization procedure is demonstrated in Figure 6 below.

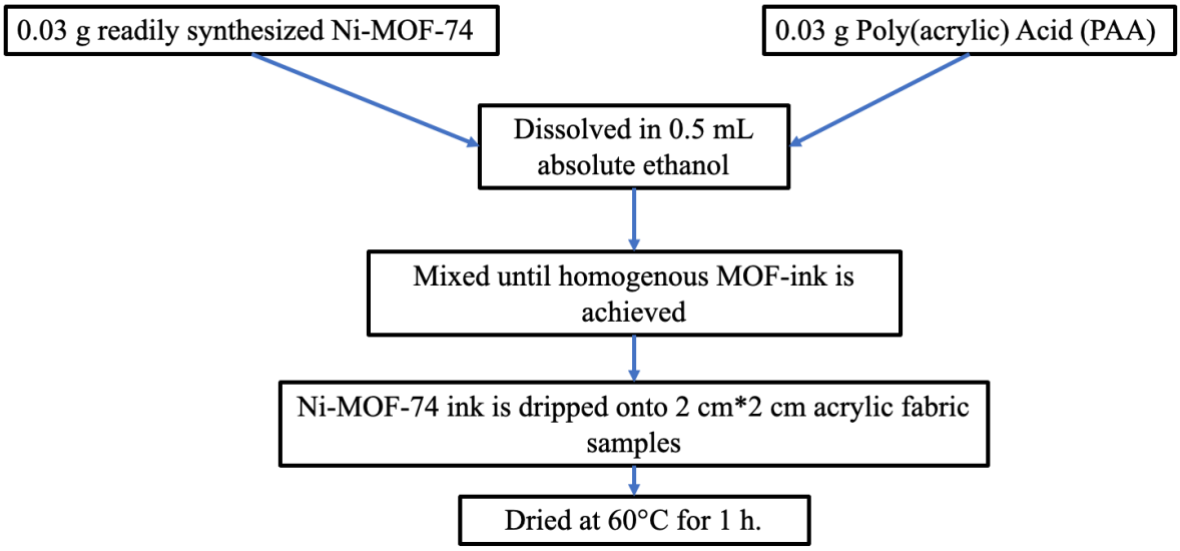

Figure 6. Procedure for the Drip Casting Method

4.4. Characterization Techniques

Morphologic structures of the synthesized Ni-MOF-74 crystals as well as the Ni-MOF-74 deposited acrylic fabrics were investigated by scanning electron microscope (SEM, FEI QUANTA 250 FEG) with different magnifications. Secondary electron (SE) and backscatter electron (BSE) detectors were utilized for SEM characterization.

The thermal stability of Ni-MOF-74 was determined by thermogravimetric analysis (Shimadzu TGA-51) with a 10°C/min heating rate in a nitrogen atmosphere at a flow rate of 40 ml/min. Fourier Transform Infrared spectrophotometer (FTIR, Shimadzu 8201) was utilized in order to determine the interaction between atoms and determination of bounded groups of the synthesized Ni-MOF-74 crystals. For the FTIR analysis, a wavelength range of 400-4000 cm^{-1} was applied. The crystallographic structure of the synthesized Ni-MOF-74 sample was investigated by X-ray diffraction (XRD, Philips X'Pert Pro Diffractometer) with a scan speed of 2°/min.

4.5. Adsorption Measurements

Adsorption studies were carried out in order to determine the CO_2 adsorption capacity of both MOF crystals and MOF-deposited fabrics. Adsorption and desorption isotherms of synthesized Ni-MOF-74 crystals as well as the Ni-MOF-74 deposited acrylic fabrics were carried out by using a volumetric adsorption instrument (Micromeritics ASAP 2010 M) under 273,150 K. 273,15 K was chosen as the analysis temperature as this temperature allows to assess the highest CO_2 capture capacity of the Ni-MOF-74. Before the adsorption measurements, samples were degassed at 200°C based on the TGA analysis of each sample in order to evacuate any trapped solvent particles in the porous structure of Ni-MOF-74. The surface areas were determined by the Langmuir method based on the data obtained from adsorption isotherms.

CHAPTER 5

RESULTS AND DISCUSSION

5.1. Structural and Morphological Characterization of Ni-MOF-74

Ni-MOF-74 powders were synthesized using the procedures laid out in Figure 3 (for MOF-74(1:1)) and Figure 4 (MOF-74(2:1)). Both procedures resulted in the successful synthesis of Ni-MOF-74. The resulting Ni-MOF-74 powder shows a yellowish-brown appearance and fine particle structure which is in line with the commercially available Ni-MOF-74 products (Chemsoon, n.d.). Structural and morphological characterization of the synthesized Ni-MOF-74 powders was conducted in order to get a better understanding of the material properties as well as to ensure that synthesis was achieved successfully.

Figure 7. As synthesized Ni-MOF-74 powder (MOF-74(1:1))

5.1.1. XRD Analysis of Synthesized Ni-MOF-74 Powders

The XRD patterns of synthesized Ni-MOF-74 samples are shown in Figure 8 and Figure 9 below in order to get an understanding of the crystallographic structure of the Ni-MOF-74 powders. For both samples, two main peaks are observed in the XRD analysis which closely correspond to the characteristic peaks (6.5° and 11.7° 2Θ for MOF-74(1:1); 7°C and 12° 2Θ for MOF-74(2:1)) for Ni-MOF-74, as reported in the literature (Wu et al. 2013; C. Chen et al. 2019). These characteristic peaks are attributed to reflection from the (1 1 0) and (3 0 0) planes (Rezaei et al. 2017a). The XRD pattern of MOF-74(2:1) shows increased noise which could be the result of instrumental effects or physical properties of the sample.

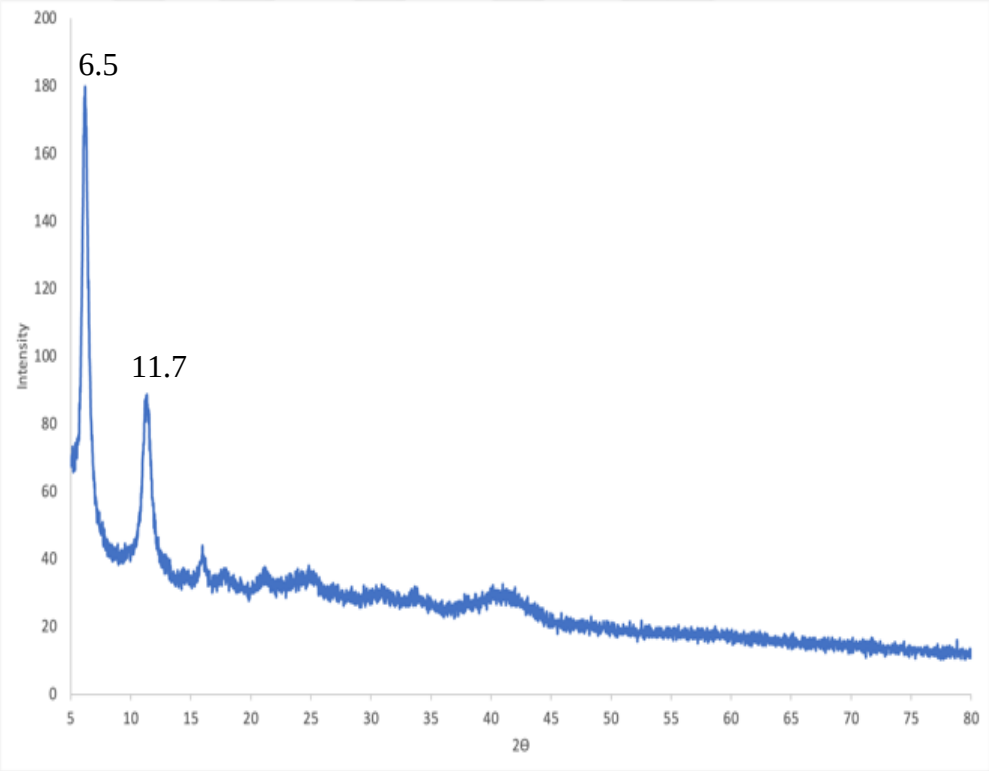

Figure 8. XRD of Ni-MOF-74 powders MOF-74(1:1)

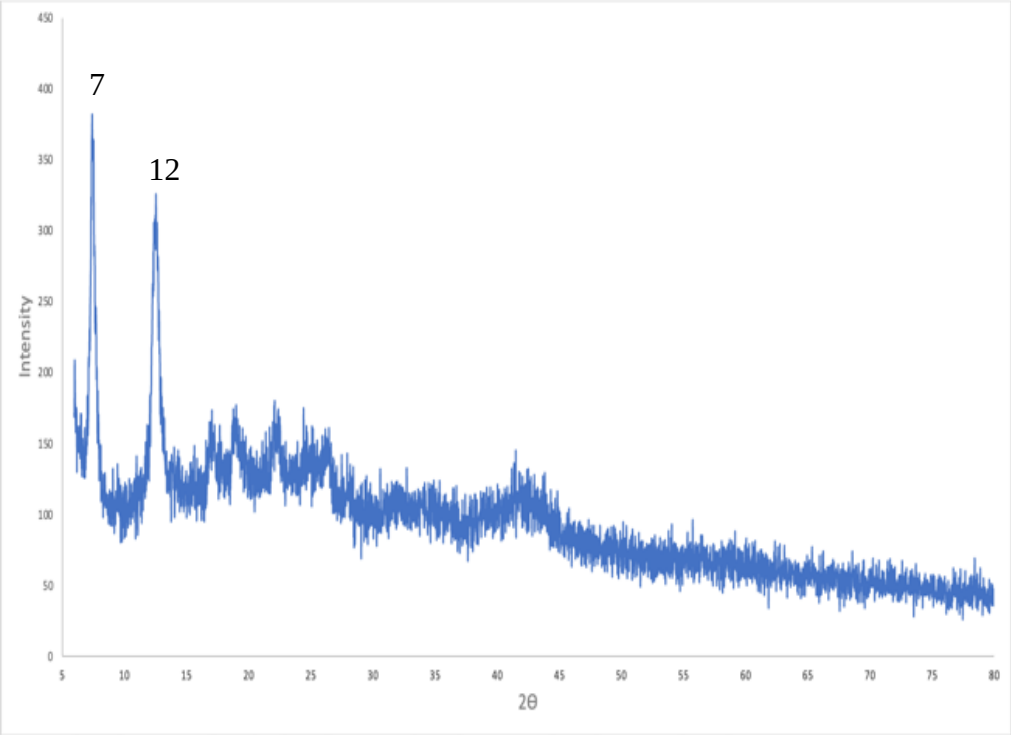

Figure 9. XRD of Ni-MOF-74 powders MOF-74(2:1)

5.1.2. FTIR Analysis of Synthesized Ni-MOF-74 Powders

The organic chemical structure and characteristics of MOF-74 samples were investigated through FTIR analysis. FTIR profiles for MOF-74(1:1) and MOF-74(2:1) are given below (Figure 10 and Figure11, respectively). For the MOF-74(1:1), the FTIR spectra show characteristic peaks at 1,555 cm^{-1} and 1,407 cm^{-1} which are attributed to symmetric and asymmetric stretching of carboxylate groups, respectively (Stuart 2004). These stretchings are found to be related to DOT linkers in the MOF-74 structure (Kamal et al. 2020). FTIR peaks located at 1,115 cm^{-1} are attributed to in-plane C-H bending while peaks at 810 and 583 cm^{-1} are attributed to out-of-plane C-H bending (Stuart 2004). The FTIR spectra of MOF-74(2:1) show a significantly similar pattern with peaks at 1,552, 1,407, 1,116, 809, and 575 cm^{-1}.

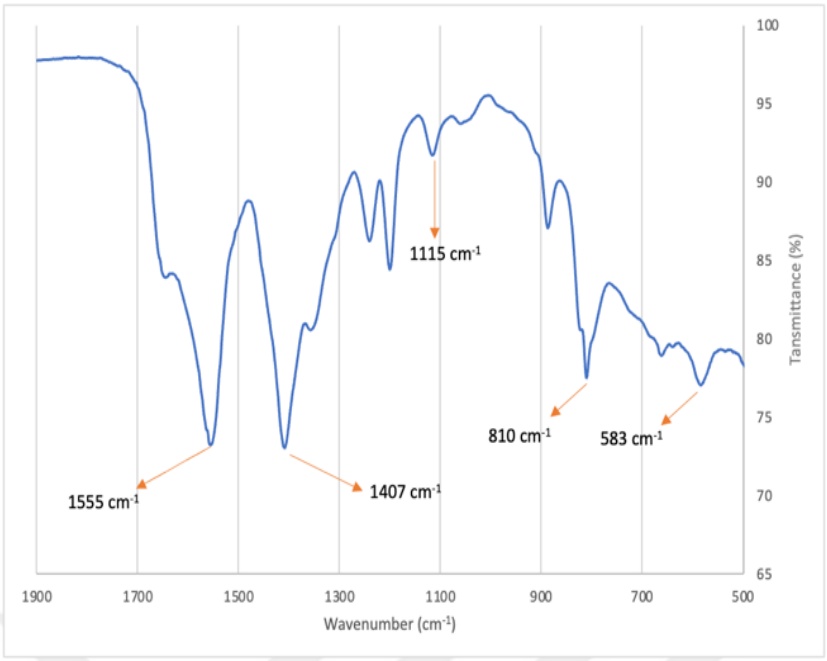

Figure 10. FTIR patterns for MOF-74(1:1)

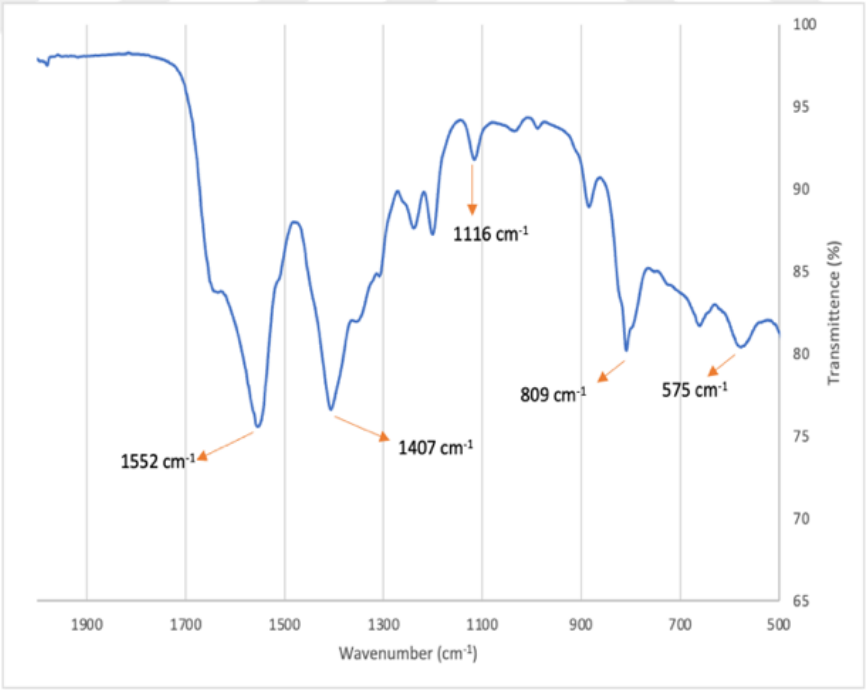

Figure 11. FTIR patterns for MOF-74(2:1)

5.1.3. SEM of Ni-MOF-74 Powders

High-resolution imaging and detailed surface examination of Ni-MOF-74 samples were carried out through scanning electron microscopy results of which are given below (Figure 12(a) and (b) for MOF-74(1:1), Figure 13(a) and (b) for MOF-74(2:1)). Investigated at a scale of 1 µm, 2 µm, and 10 µm, SEM images of synthesized Ni-MOF-74 powders reveals a rice-like structure for MOF-74(1:1) which is consistent with the reported literature (C. Chen et al. 2019).

On the other hand, MOF-74(2:1) particles show a smoother surface structure which could be a result of incomplete activation or unreacted metal salt. It is observed that MOF particles are present in clusters for both samples (Figure 12(c) and Figure 13(c)). This cluster formation can be attributed to impurities such as DMF trapped in the structure or unreacted DOT.

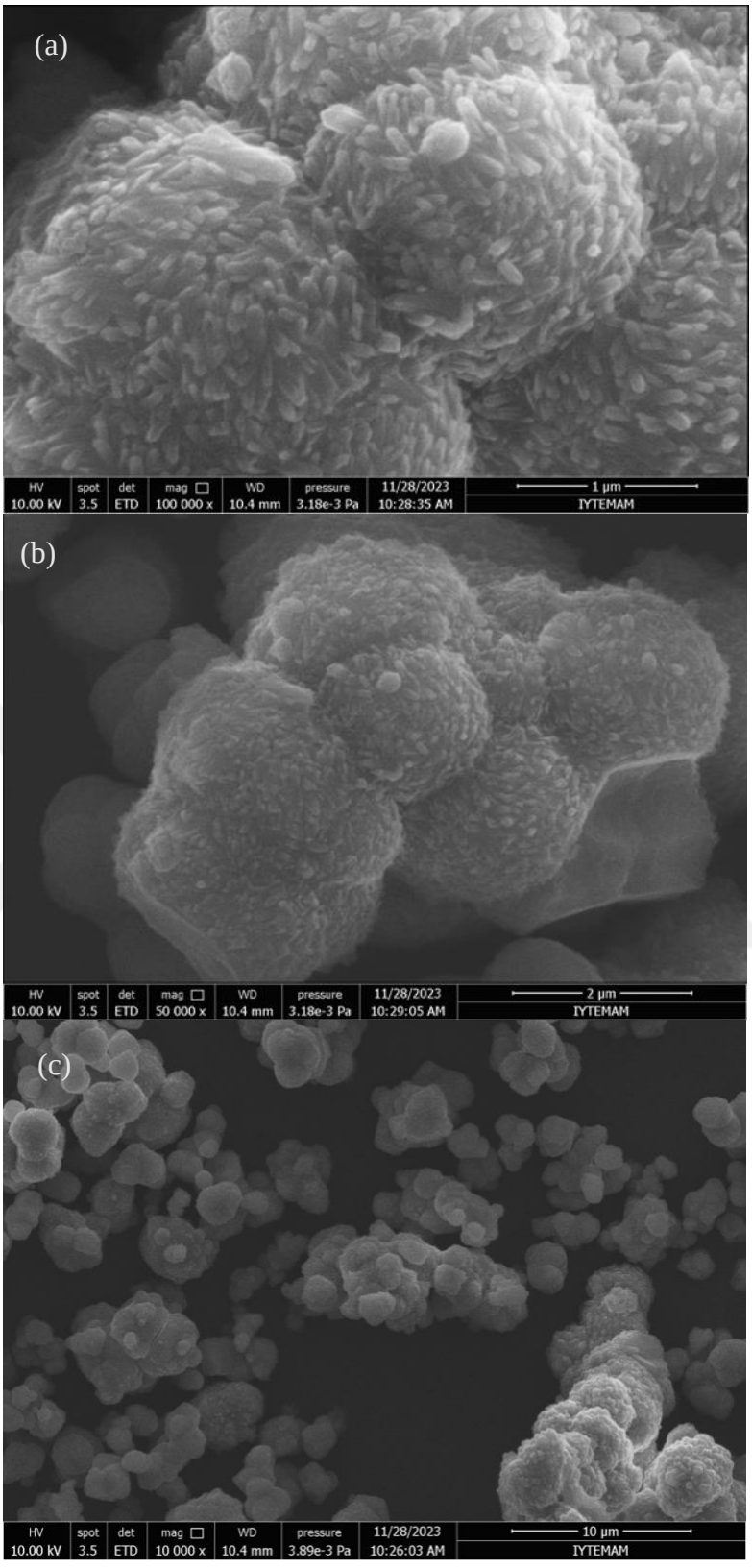

Figure 12. SEM images for MOF-74(1:1) at a scale of (a) 1 µm with 100,000 x, (b) 2 µm with 50,000 x, and (c) 10 µm with 10,000 x

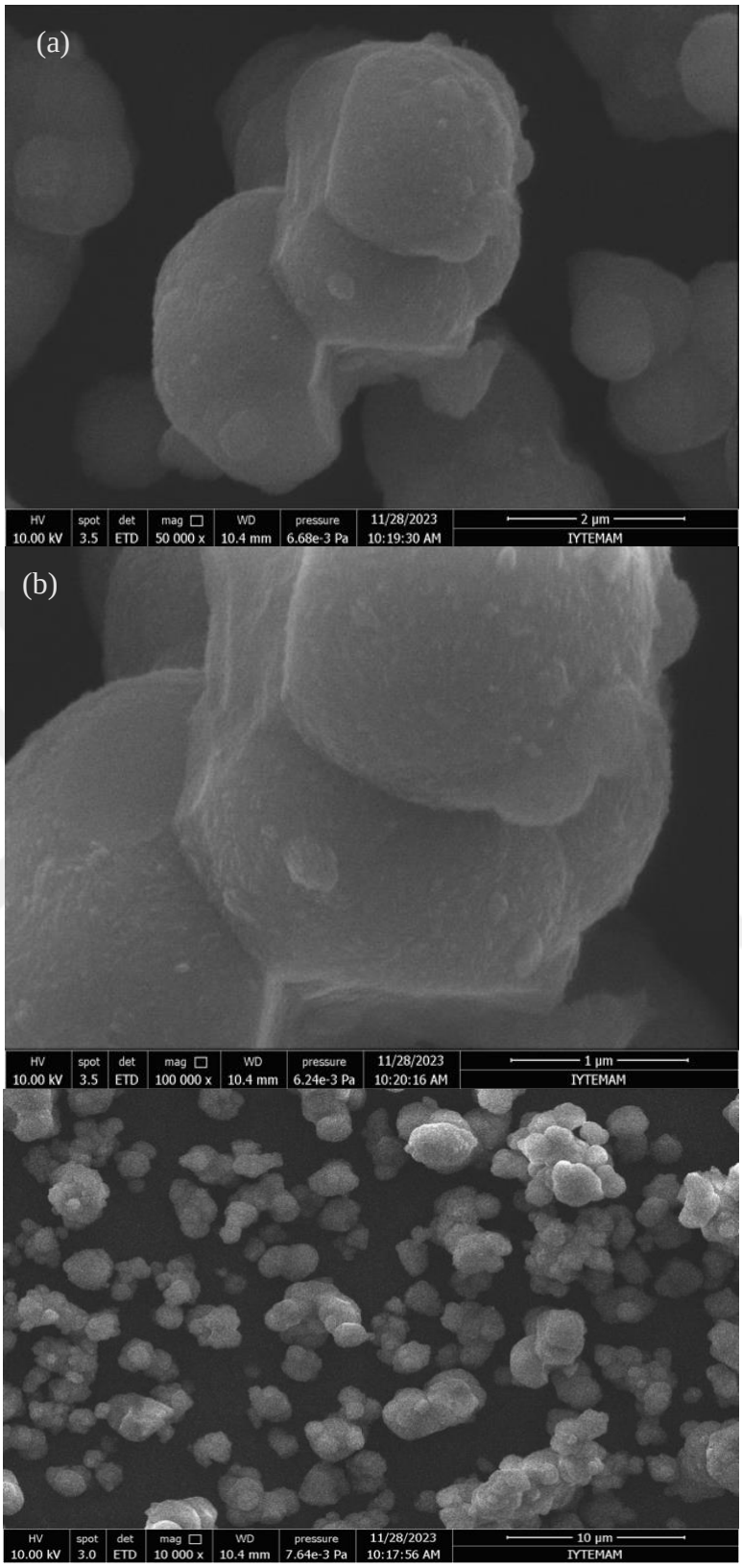

Figure 13. SEM images for MOF-74(2:1) at a scale of (a) 1 µm with 100,000 x (b) 2 µm with 50,000 x, and (c) 10 µm with 10,000 x

5.1.4. TGA of Synthesized Ni-MOF-74 Powders

The thermogravimetric analysis of MOF-74 samples results in a similar profile for both MOF-74(1:1) and MOF-74(2:1). The initial weight loss at around 100-150°C can be attributed to loss of trapped solvents in the structure while the 400°C point marks the complete structural collapse. This information is then used as the reference temperature for degassing applications before the adsorption experiments.

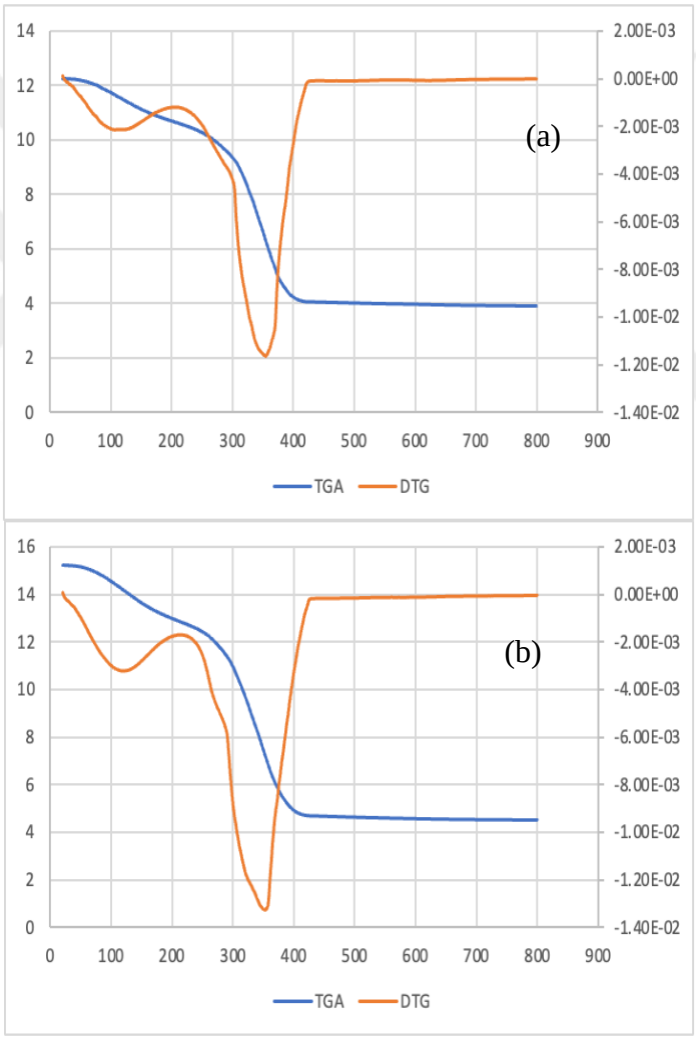

Figure 14. TGA analysis results for (a) MOF-74(1:1) and (b) MOF-74(2:1)

5.2. CO_2 Adsorption Capacities

In order to investigate the adsorption behavior and pore textural properties of synthesized Ni-MOF-74 powders and Ni-MOF-74 immobilized on acrylic fabrics, adsorption experiments were conducted. To this end, adsorption experiments were carried out under a CO_2 (at 273 K) environment.

Adsorption isotherms, Langmuir surface area, and pore properties of the synthesized Ni-MOF-74 powders as well as Ni-MOF-74 immobilized on acrylic fabrics were investigated.

5.2.1. CO_2 Adsorption and Desorption Isotherms of Ni-MOF-74

Langmuir surface area, adsorption and desorption isotherms as well as fit of experimental data to adsorption models for MOF-74(1:1) and MOF-74(2:1) powders are investigated based on the fitting of experimental data to the Langmuir model. A summary of surface area analysis is given in Table 4 below.

Table 4. Langmuir Surface Areas of MOF-74(1:1) and MOF-74(2:1)

	Langmuir surface area (m^2/g)
MOF-74(1:1)	180
MOF-74(2:1)	114

It is observed that MOF-74(1:1) shows a slightly higher surface area than MOF-74(2:1) which was also reflected in the SEM images of the samples. MOF-74(2:1) showed a smoother surface in comparison to MOF-74(1:1). On the other hand, Ni-MOF-74 powders synthesized in this work showed significantly lower Langmuir surface areas. This can be a result of unreacted organic ligands, unreacted metal salts, or solvent material

trapped inside the porous structure. In order to achieve a higher surface area, the activation or washing process should be optimized.

Adsorption and desorption isotherms for MOF-74(1:1) and Ni-MOF(2:1) are demonstrated in Figure 15 and Figure 16 below, respectively. As it is apparent from the isotherms, the adsorption behavior of the Ni-MOF-74 powders follows a Type I isotherm (IUPAC 1985).

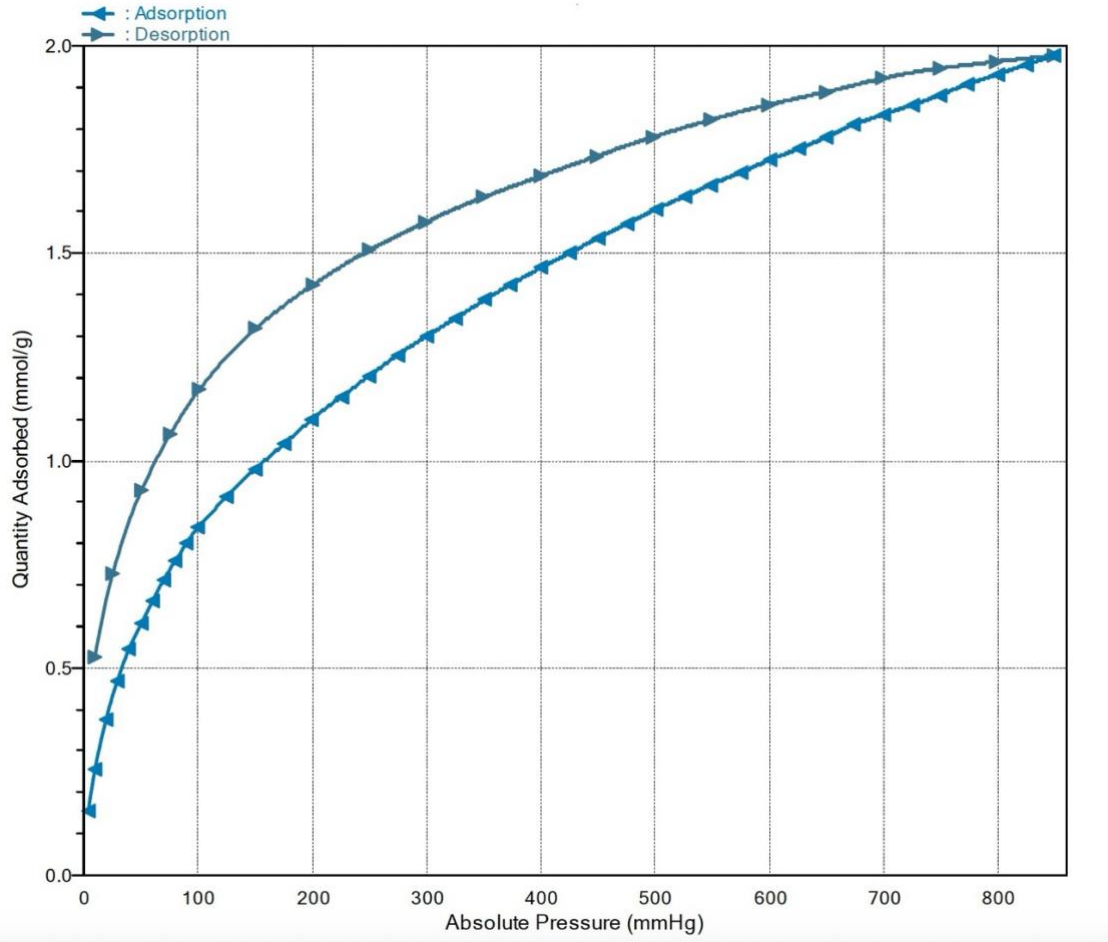

Figure 15. Adsorption and desorption isotherms for MOF-74(1:1)

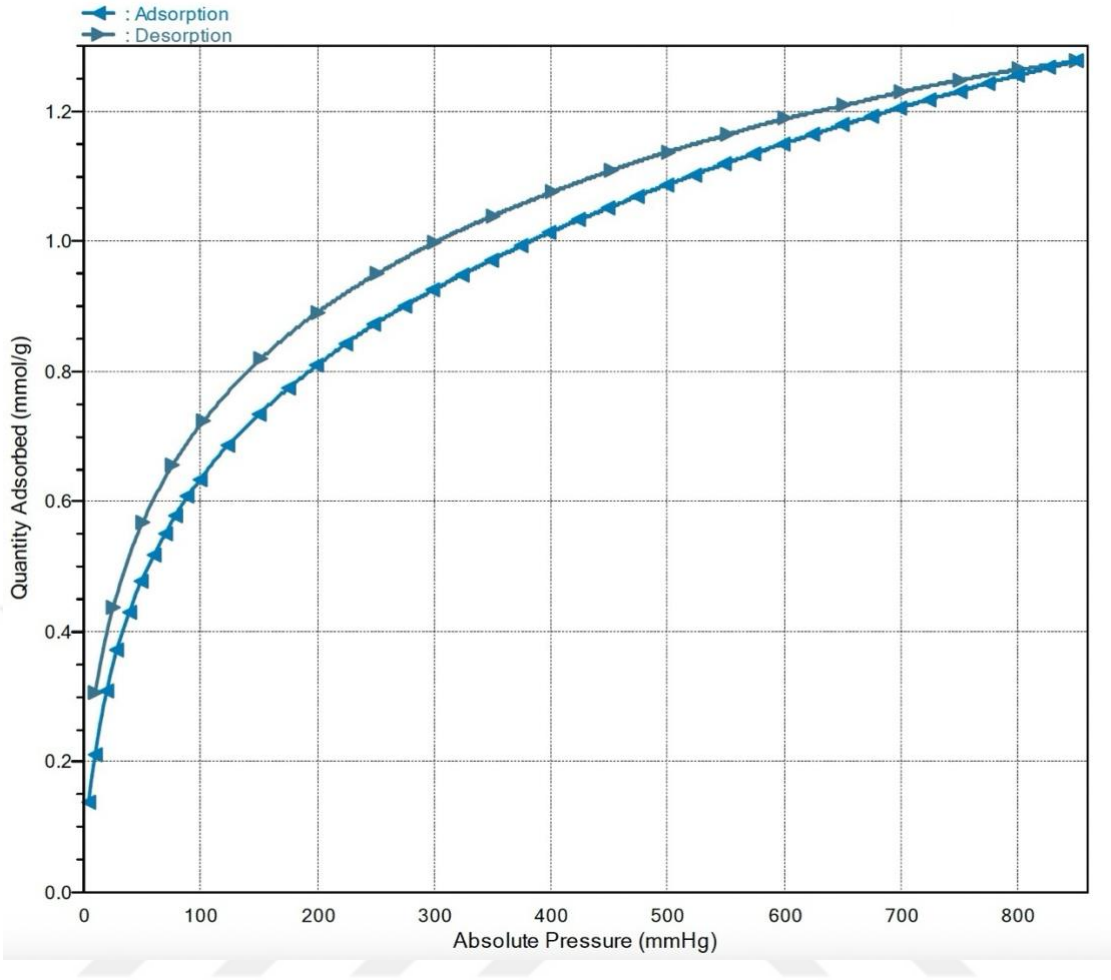

Figure 16. Adsorption and desorption isotherms for MOF-74(2:1)

The adsorption analysis reveals that MOF-74(1:1) powder shows a higher adsorption capacity (1.98 mmol/g) than MOF-74(2:1) powder (1.28 mmol/g). This is attributed to physical hindrance caused by unreacted nickel salts or inefficient activation of the MOF-74(2:1) sample.

In order to evaluate the adsorption behavior of Ni-MOF-74 powders, it is important to fit experimental adsorption data to adsorption isotherm models. For this study, Langmuir and Freundlich models were investigated. Langmuir and Freundlich fittings for the MOF-74(1:1) sample are given in Figure 17 and Figure 18, respectively.

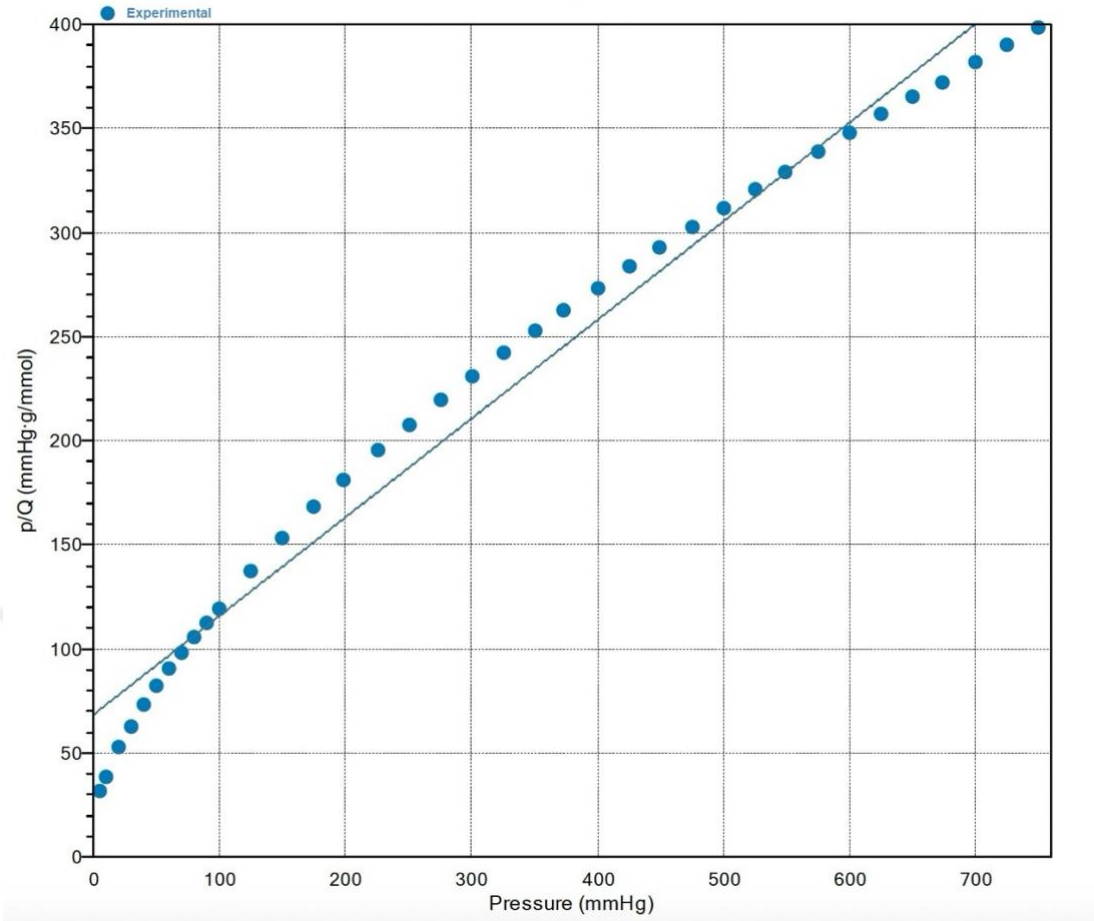

Figure 17. Langmuir adsorption isotherm of MOF-74(1:1)

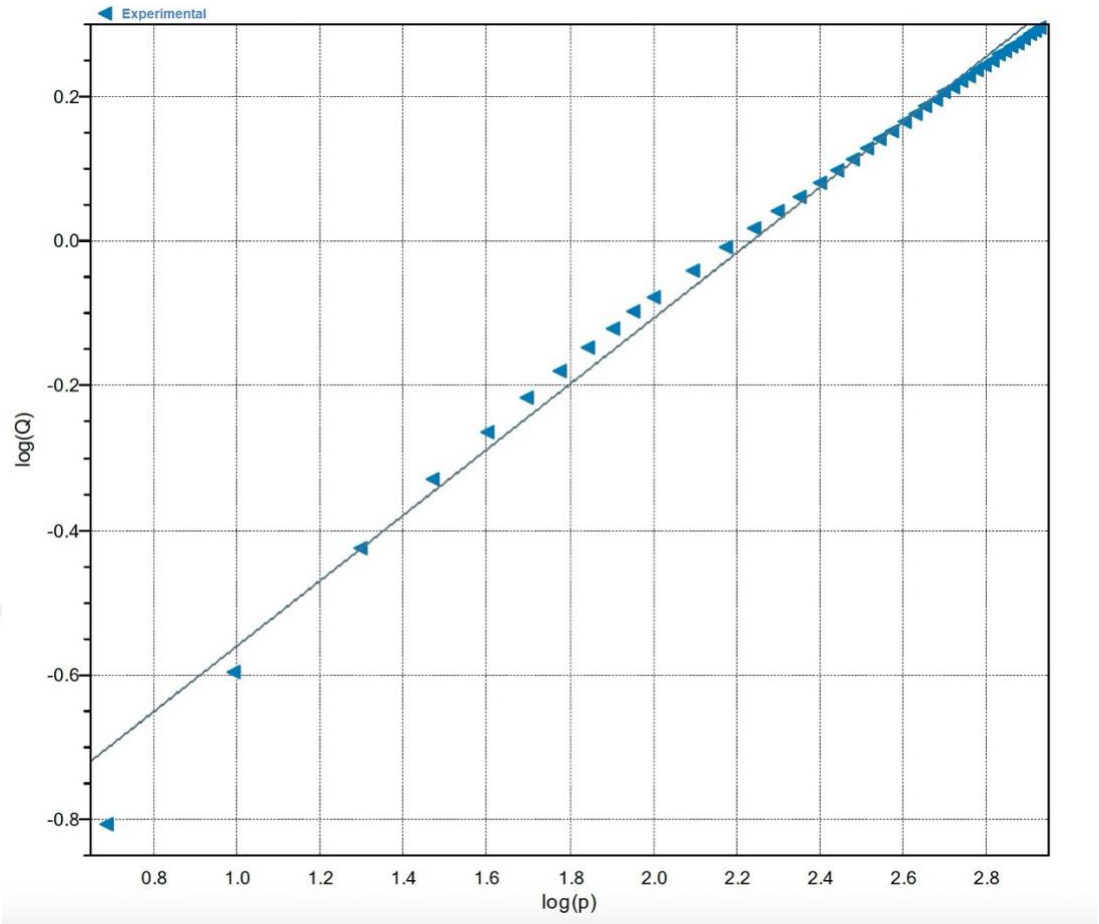

Figure 18. Freundlich adsorption isotherm of MOF-74(1:1)

Table 5. CO_2 Adsorption Parameters for MOF-74(1:1)

Parameters Langmuir isotherm	**Langmuir isotherm**	**Parameters Freundlich**	**Freundlich isotherm**
Temperature(k)	273.15	**Temperature(k)**	273.15
Qm (mmol/g)	2.11067	**Qm.C (mmol/g)**	0.0968
b	0.006923	**n**	2.205
R	0.989240	**R**	0.95730

Langmuir and Freundlich models for MOF-74(2:1) sample are given in Figure 19 and Figure 20, respectively.

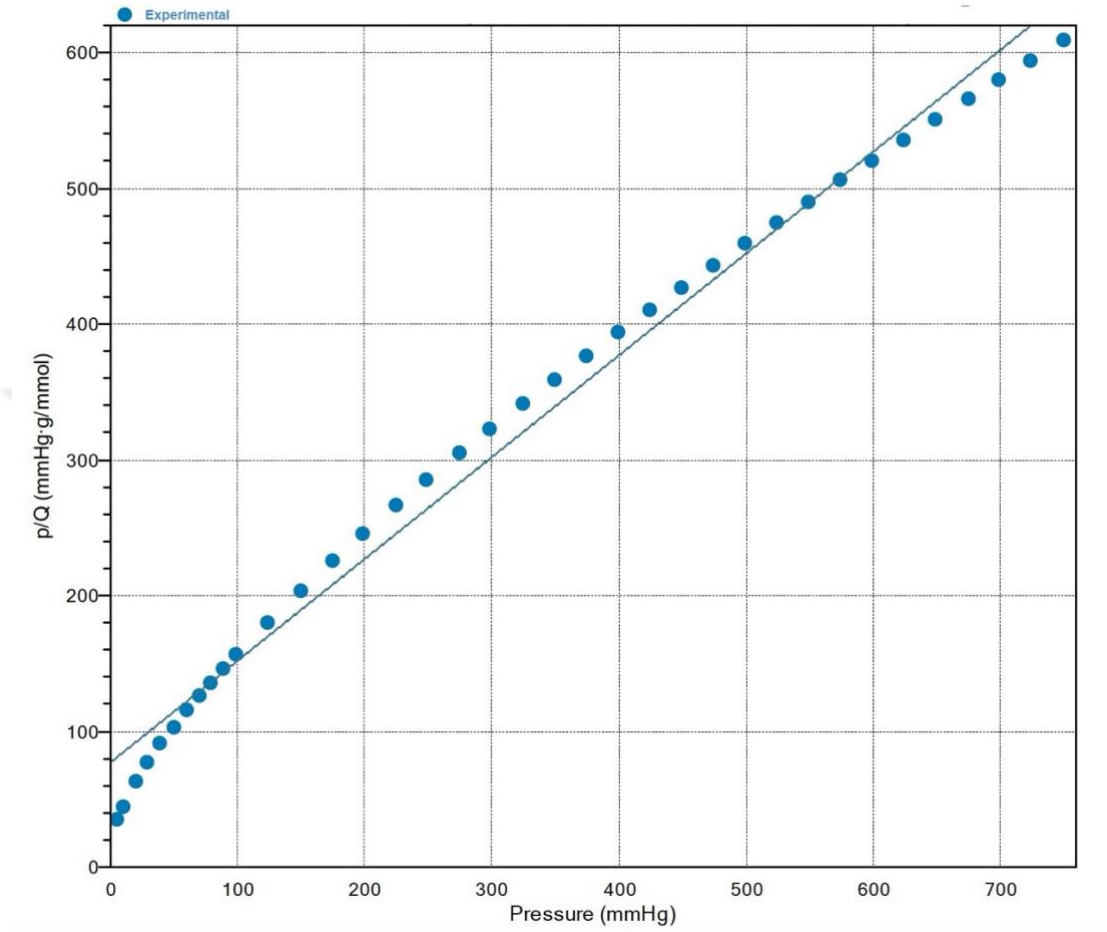

Figure 19. Langmuir adsorption isotherm of MOF-74(2:1)

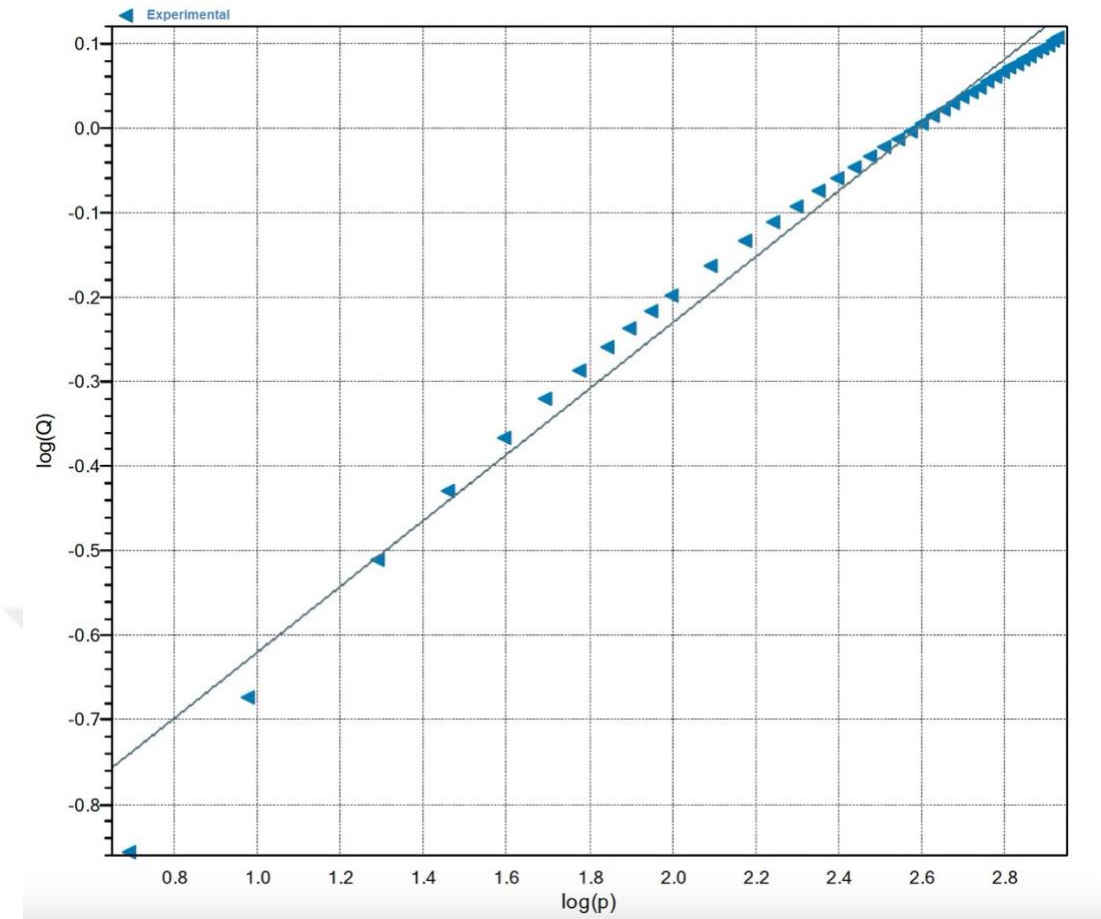

Figure 20. Freundlich adsorption isotherm of MOF-74(2:1)

Table 6. CO_2 Adsorption Parameters for MOF-74(2:1)

Parameters Langmuir isotherm	**Langmuir isotherm**	**Parameters Freundlich**	**Freundlich isotherm**
Temperature(k)	273.15	**Temperature(k)**	273.15
Qm (mmol/g)	1.33333	**Qm.C (mmol/g)**	0.0977
b	0.00974	**n**	2.5655
R	0.994493	**R**	0.99207

For MOF-74(1:1), the experimental adsorption data presents a better fit with Freundlich isotherm in comparison to Langmuir isotherm based on the correlation coefficients (r^2). Suitability to Freundlich isotherm suggests heterogenous active adsorption sites on the MOF-74(1:1) surface.

On the other hand, the experimental adsorption data presents a better fit with Langmuir isotherm in comparison to Freundlich isotherm based on the correlation coefficients (r^2). Suitability to Langmuir isotherm suggests monolayer adsorption on the MOF-74(2:1) surface.

5.3. Application on Acrylic Fabric

As it was outlined in Chapter 4 of this report, two different MOF immobilization techniques were applied in order to achieve immobilization on acrylic fabric surface. The first of these techniques was the in-situ dip coating technique in which the acrylic fabrics were immersed in the synthesis solutions during the synthesis of Ni-MOF-74 powder. However, this adopted technique failed to result in the immobilization of Ni-MOF-74 onto the fabric surface. Due to the chemical structure of the fabric and organic solvent used for synthesis (DMF) combined with the high synthesis temperature of (110°C), the fabric structure was completely disintegrated after the 24 h reaction period. The resulting acrylic fabric-MOF mixture is presented in Figure 21 below. As can clearly be seen from the figure, the fabric structure was completely decomposed.

Figure 21. Decomposed fabric structure after in-situ dip coating process

However, the second immobilization method, drip casting, resulted in the successful immobilization of as-synthesized Ni-MOF-74 powder (MOF-74(1:1)). The Drip casting process and resulting MOF-coated acrylic fabric (ATIII) is demonstrated in Figure 22.

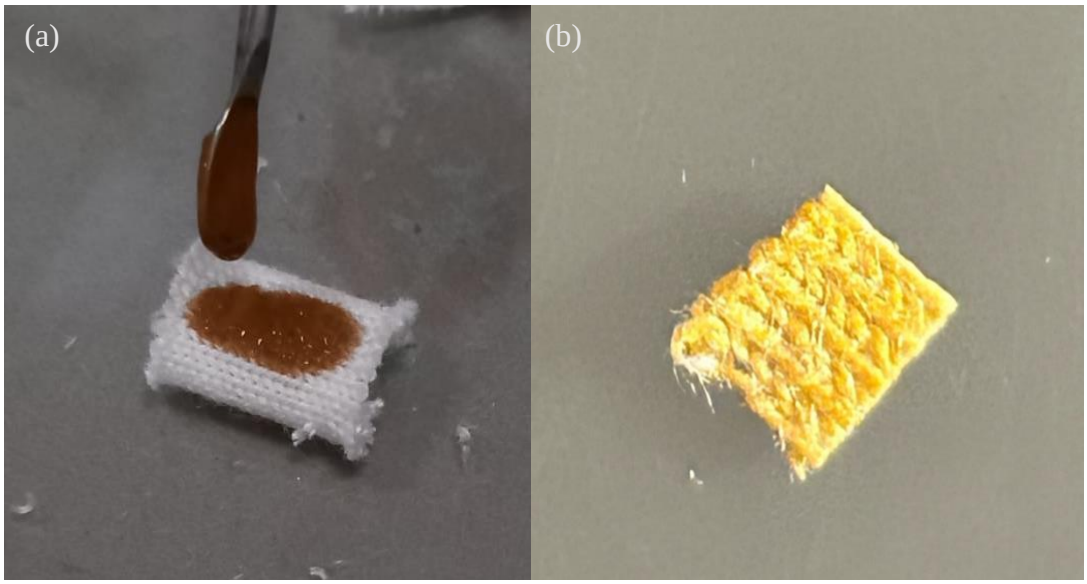

Figure 22. (a) drip casting method and (b) acrylic fabric coated with Ni-MOF-74

Figure 22(a) demonstrates the drip casting process with the prepared MOF-ink while Figure 22(b) demonstrates the final product after drying the coated fabric. The initial confirmation of MOF immobilization is indicated by the color change of acrylic fabric from white to yellowish-brown.

5.3.1. SEM of Ni-MOF-74 Coated Acrylic Fabric

In order to further investigate the immobilization of Ni-MOF-74 on an acrylic fabric surface scanning electron microscopy method was applied. Figure 23 below shows the SEM images of MOF-coated acrylic fabric sample (ATIII) at a scale of 100 µm and 50 µm. Figure 23(a) demonstrates that MOF-ink penetrated through the woven fabric and immobilized on the individual fibers. The coating of Ni-MOF-74 can be seen more clearly in Figure 23(b).

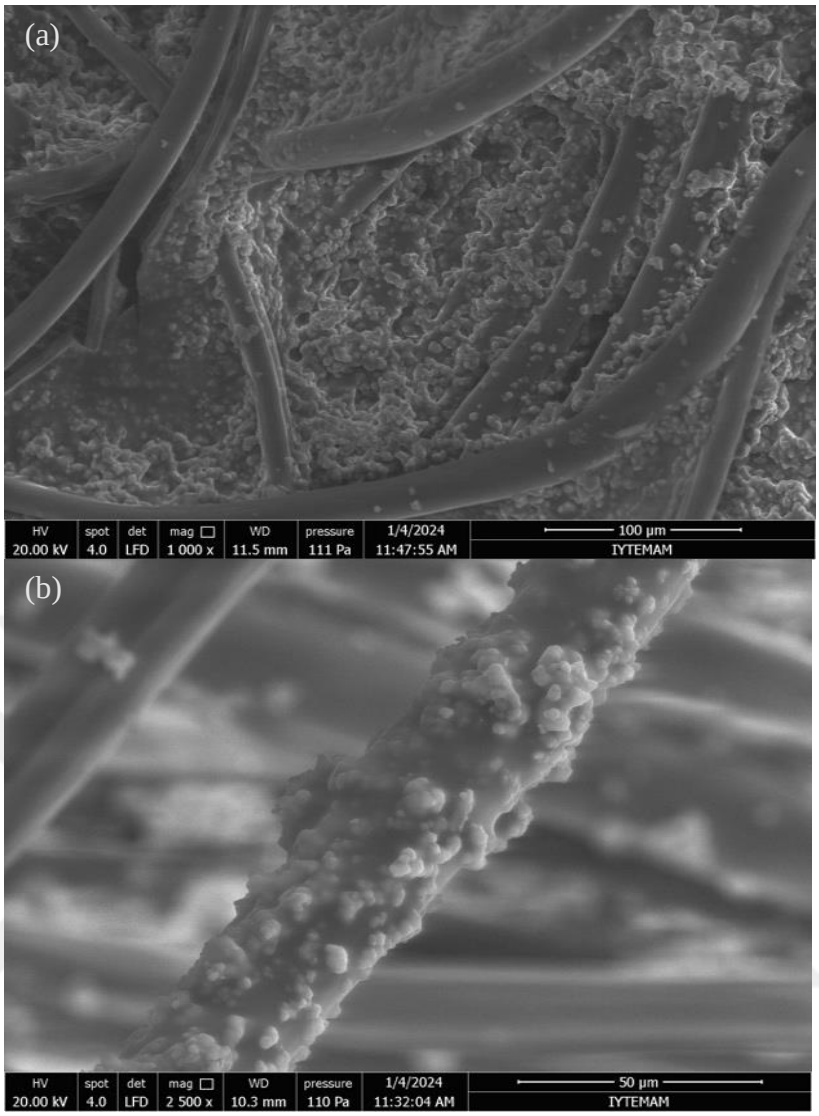

Figure 23. SEM images of Ni-MOF-74 immobilized acrylic fabric at a scale of (a) 100 µm at 1,000 x and (b) 50 µm at 2,500 (ATIII)

Figure 24 below shows the SEM images of MOF-coated acrylic fabric sample (ATIII) at a scale of 100 µm and 50 µm. These SEM images present MOF-ink penetration through the fabric structure and gives a closer look into the MOF coting on fibers

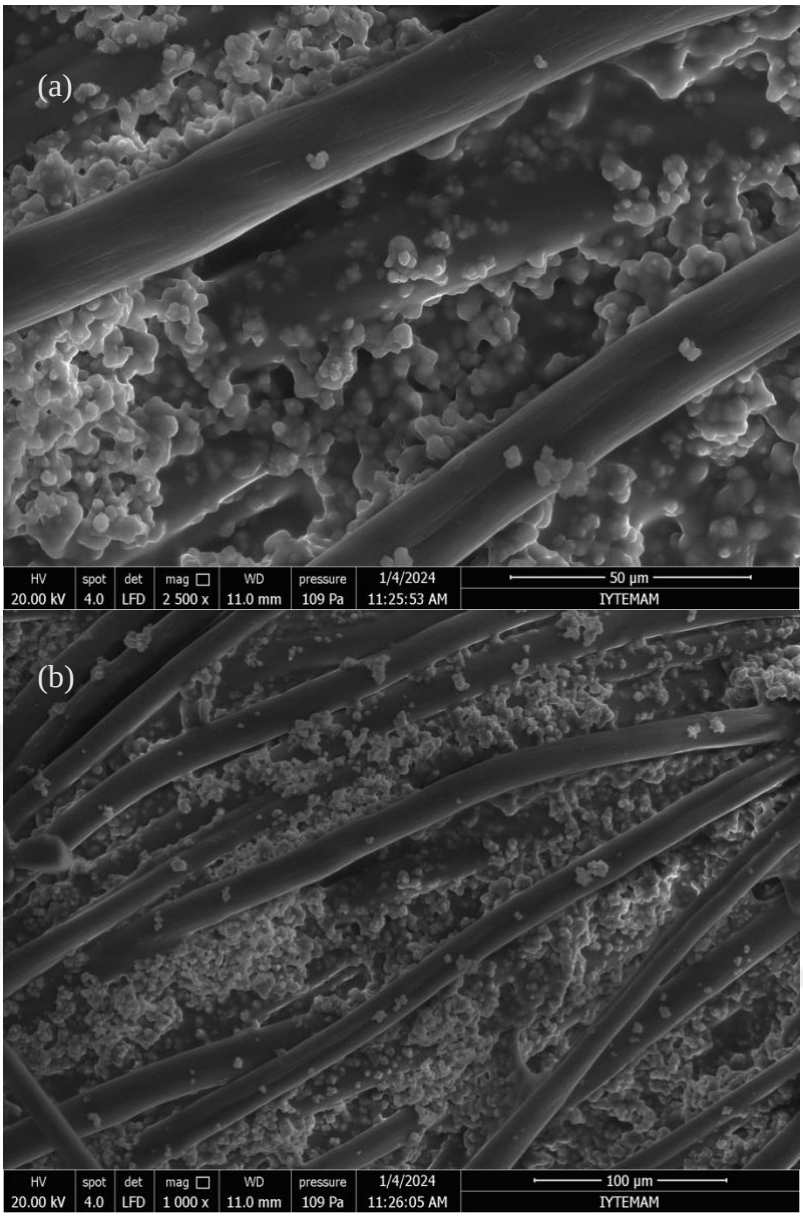

Figure 24. SEM images of Ni-MOF-74 immobilized acrylic fabric at a scale of (a) 50 µm at 2,500 x and (b) 100 µm at 1,000 (AK700)

These SEM images prove the successful immobilization of Ni-MOF-74 on acrylic fabrics for the first time. However, agglomeration of Ni-MOF-74 particles to a degree can be observed on the fiber surface. Furthermore, PAA is clearly observed between and around the MOF particles resembling a filler material.

5.3.2. TGA of Ni-MOF-74 Coated Acrylic Fabric

Thermogravimetric analysis for both samples were also performed. The results show similar thermogravimetric behavior for both Ni-MOF-74 immobilized ATIII and AK700 samples. Thermogravimetric analyses of MOF-coated acrylic fabrics show a two-step mass loss, one of which is observed at around 400°C while the other is observed at around 600°C. Mass loss at 400°C is attributed to the decomposition of the Ni-MOF-74 structure immobilized on the fabric surface as it corresponds with the TGA curves of synthesized Ni-MOF-74 powders. Consequently, mass loss at 600°C is attributed to the complete decomposition of the fabric structure itself. This information is then used as the reference temperature for degassing applications before the adsorption experiments.

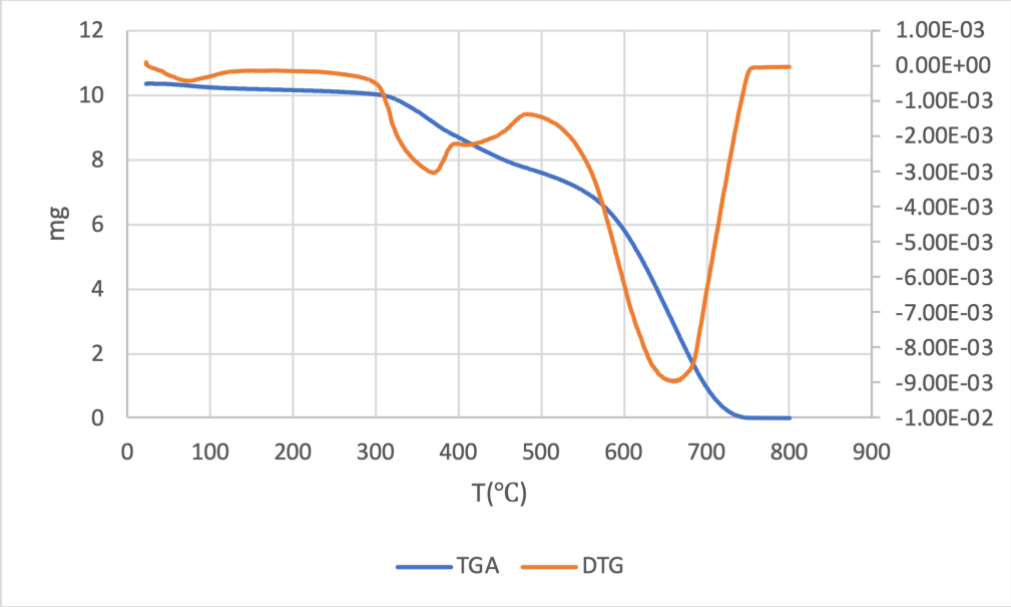

Figure 25. TGA analysis results Ni-MOF-74 immobilized acrylic fabric (ATIII)

Figure 26. TGA analysis results Ni-MOF-74 immobilized acrylic fabric (AK700)

5.3.3. CO_2 Adsorption Capacity of Ni-MOF-74 Coated Acrylic

Immobilizing Ni-MOF-74 onto acrylic fabric opens the way to practical applications of Ni-MOF-74 for CO_2 capture. However, in order to investigate the effect of immobilization on the CO_2 adsorption capacity of the synthesized MOF material, an adsorption analysis must be done. To this end, adsorption studies under a CO_2 environment were conducted. The adsorption capacity of MOF-74(1:1) coated fabric (ATIII) with a smoother surface structure was measured as 1.82 mmol/g which is slightly lower than the synthesized Ni-MOF-74 powder (MOF-74(1:1)) at 1.98 mmol/g. This decrease in CO_2 adsorption capacity is attributed to the effect of polyacrylic acid (PAA) utilized for MOF-ink formation as well as the physical hindrance created by the fabric fiber at the contact surface with the MOF particles.

The experimental adsorption and desorption isotherms for MOF-74(1:1) coated fabric (ATIII) are given in Figure 27 below.

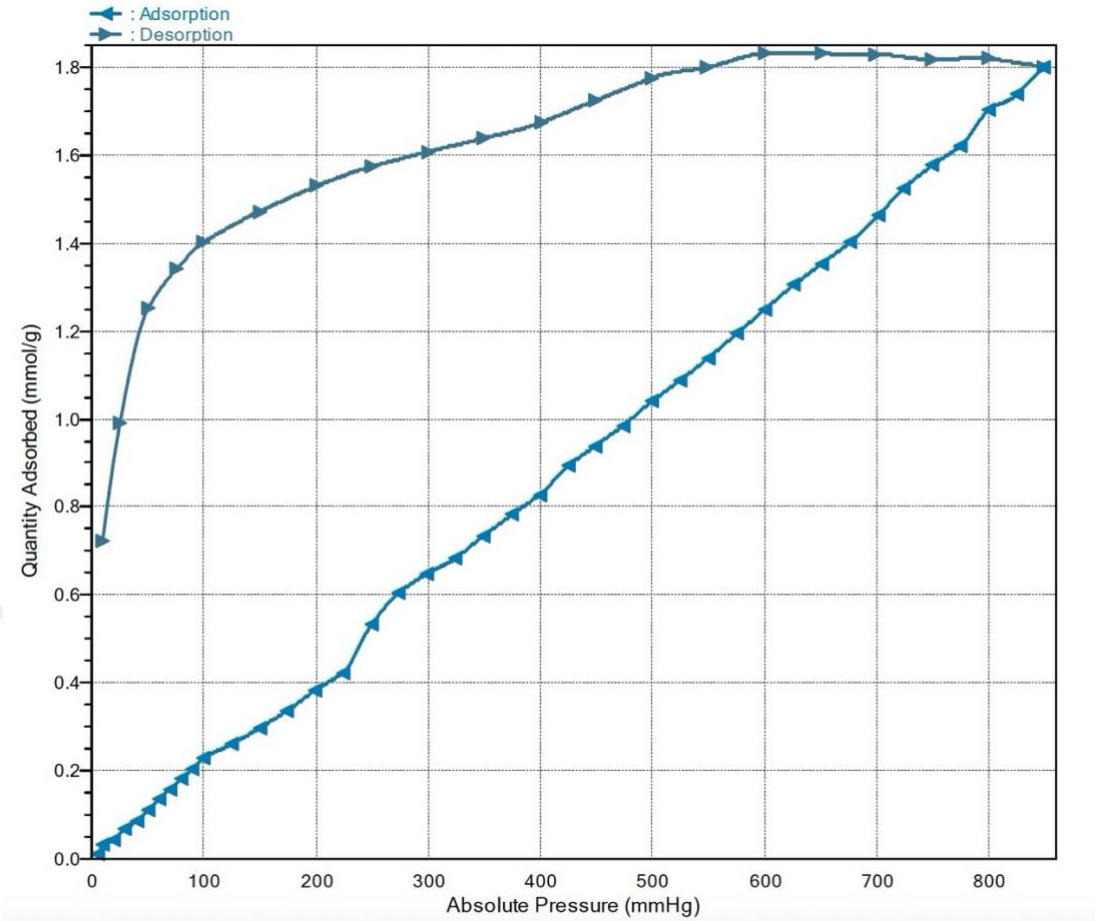

Figure 27. Adsorption and desorption isotherms for Ni-MOF-74(1:1) immobilized acrylic fabric (ATIII)

It is observed that desorption isotherm shows a similar form to synthesized Ni-MOF-74 powder. On the other hand, the adsorption isotherm shows a different form than the adsorption isotherm of MOF-74(1:1). This is attributed to the effect of polyacrylic acid (PAA) utilized for MOF-ink formation, the increased heterogeneity of adsorbent surface, as well as agglomeration of MOF particles on fabric fibers. Such effects clearly resulted in an irregular adsorption isotherm that most similarly resembles Type III in the Brunauer classification of isotherms. This can be tied to the increased level of complexity in the structure of interfaces due to the penetration of MOF particles into the fabric structure. Additionally, the presence of PAA in the MOF-ink is likely to be the reason for the change in the adsorption type as some of the pores might have been blocked off completely or partially creating a wide range of pore sizes. (Douglas M. Ruthven 1984).

In order to evaluate the adsorption behavior of Ni-MOF-74 coated acrylic fabrics, experimental adsorption data was fitted to adsorption isotherm models. For this study, Freundlich model was investigated. Figure 28 demonstrates the fitting to the Freundlich model while Table 7 shows adsorption isotherm parameters related to Freundlich fitting.

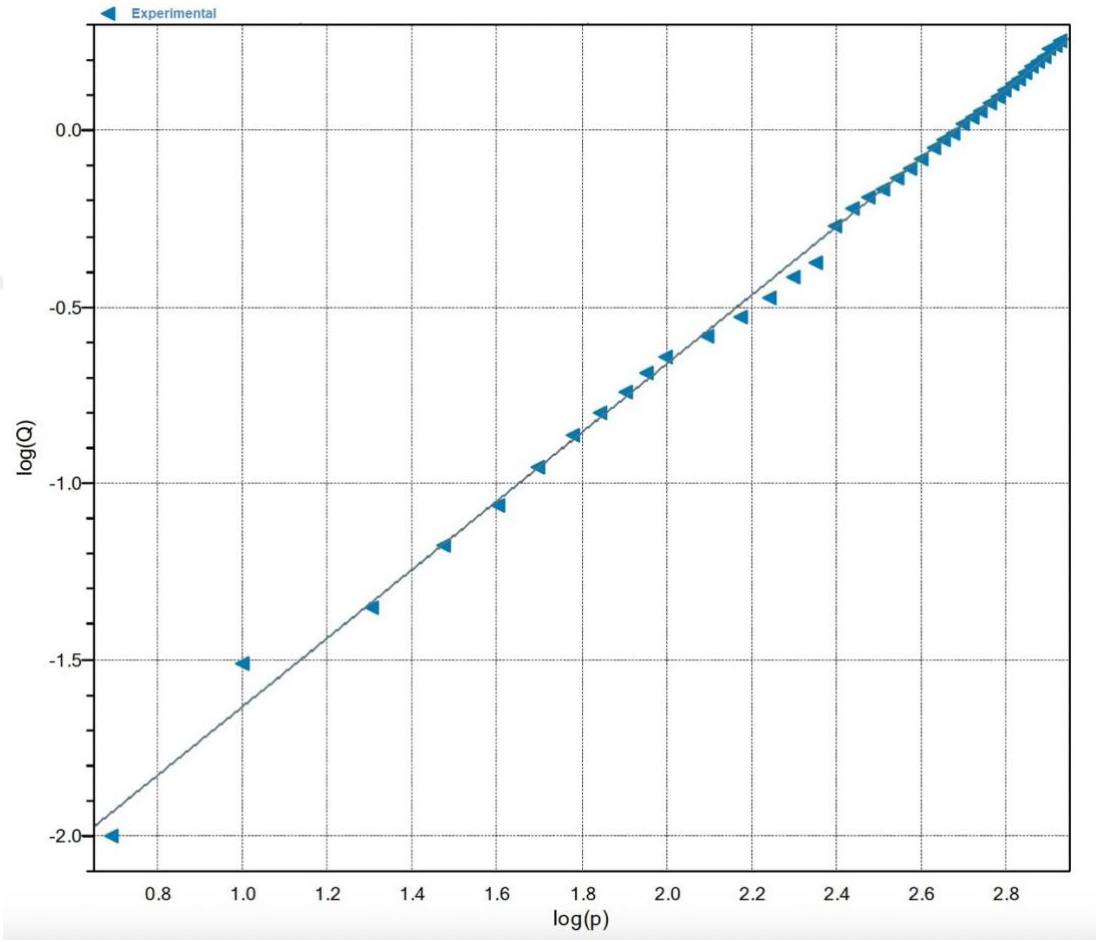

Figure 28. Freundlich adsorption isotherm of Ni-MOF-74(1:1) immobilized acrylic fabric (ATIII)

Table 7. CO_2 adsorption isotherm parameters for Ni-MOF-74 immobilized acrylic Fabric (ATIII)

Parameters Freundlich	**Freundlich isotherm**
Temperature(K)	273.15
Qm.C (mmol/g)	0.00025
n	1.0283
R	0.998675

For the Ni-MOF-74(1:1) immobilized Acrylic Fabric the Freundlich model shows a suitable fit to the experimental adsorption data based on the correlation coefficient (r^2) of 0.998675. This revelation further supports the conclusion that Ni-MOF-74(1:1) coated acrylic fibers have heterogenous adsorption sites. It can also be concluded that multilayer adsorption is observed for the MOF coated acrylic fabrics.

The immobilization study presents a significant opportunity for the practical application of Ni-MOF-74 on a flexible acrylic fabric surface. Considering that acrylic fabrics can be integrated into various real-life applications such as outdoor coverings, further investigating the opportunities for Ni-MOF-74 coated acrylic fabrics remains an interesting research area.

For the same purpose, adsorption studies for MOF coated AK700 sampled under were conducted. For MOF-74(1:1) coated fabric (AK700) with a rougher surface structure maximum adsorption capacity was measured as 0.62 mmol/g which is significantly lower than (69%) the synthesized Ni-MOF-74 powder (MOF-74(1:1)) at 1.98 mmol/g. This further decrease in CO_2 adsorption capacity is attributed to the increased effect of physical hindrance created by the fabric fiber at the contact surface with the MOF particles due to the rougher surface structure of this fabric sample as well as the effect of polyacrylic acid (PAA) utilized for MOF-ink formation.

The experimental adsorption and desorption isotherms for MOF-74(1:1) coated fabric (ATIII) are given in Figure 29 below.

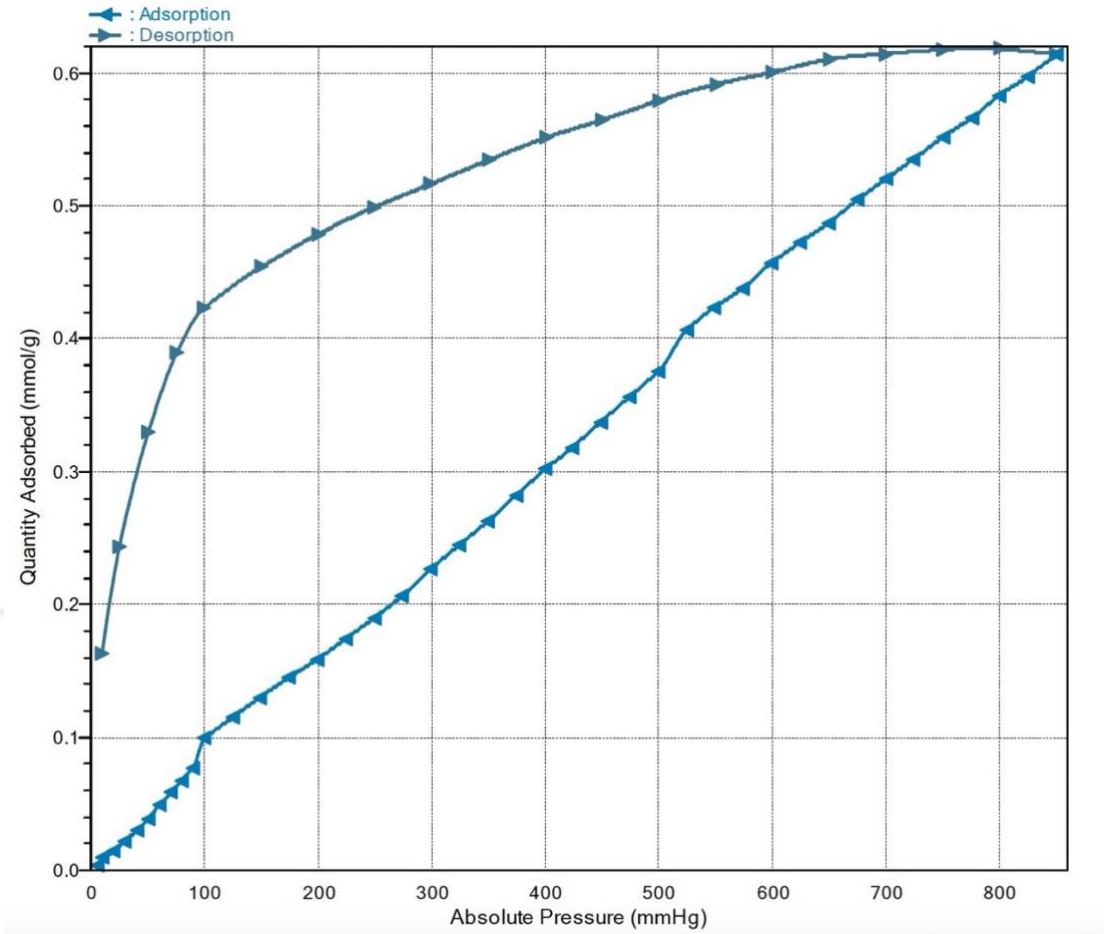

Figure 29. Adsorption and desorption isotherms for Ni-MOF-74(1:1) immobilized acrylic fabric (AK700)

Experimental adsorption data was fitted to adsorption Freundlich isotherm model. Figure 30 demonstrates the fitting to the Freundlich model while Table 8 shows adsorption isotherm parameters related to Freundlich fitting.

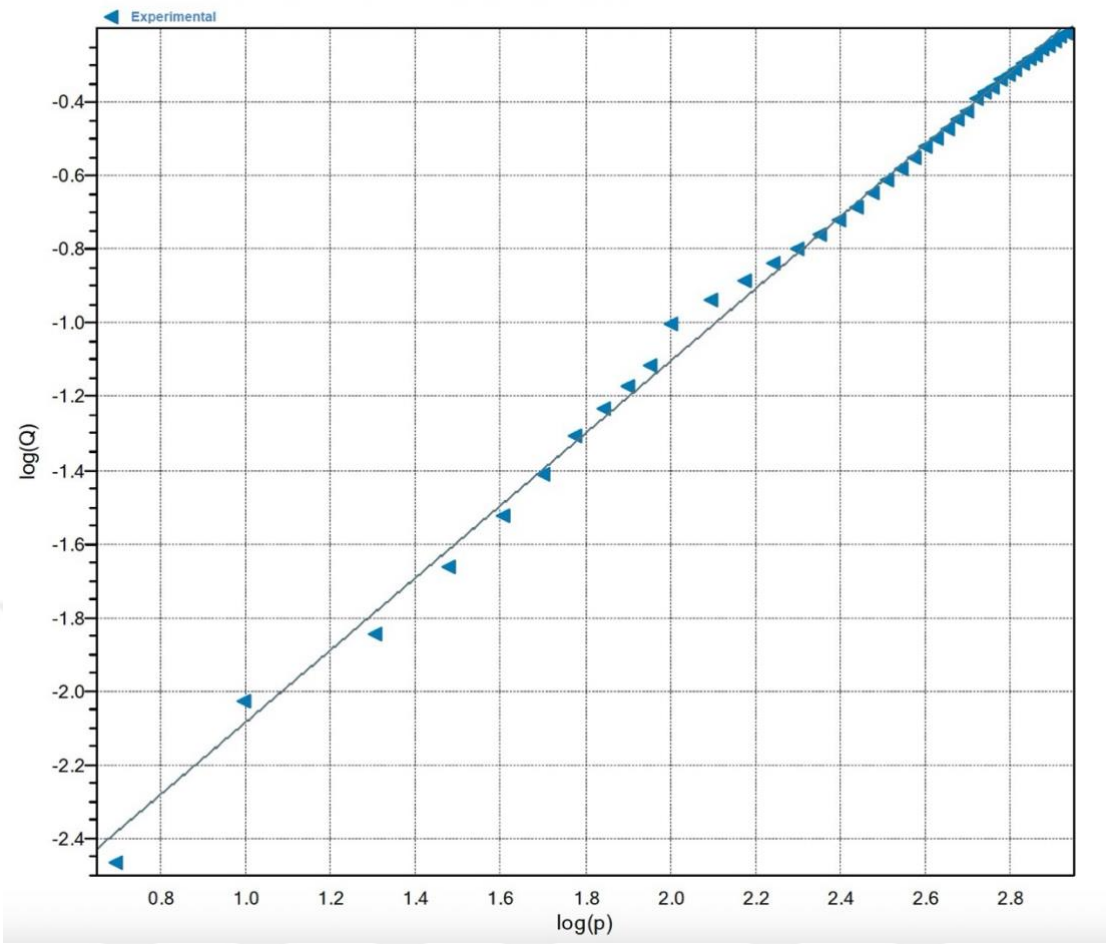

Figure 30. Freundlich adsorption isotherm of Ni-MOF-74(1:1) immobilized acrylic fabric (AK700)

Table 8. CO_2 adsorption isotherm parameters for Ni-MOF-74 immobilized Acrylic Fabric (AK700)

Parameters Freundlich	**Freundlich isotherm**
Temperature (K)	273.15
Qm.C (mmol/g)	0.0009
n	1.0197
Correlation coefficient	0.998324

5.3.4. CO_2 Adsorption Capacity of In-situ Dip Coating Sample

Despite the fact that the fabric structure was completely decomposed during the in-situ dip coating technique, the CO_2 adsorption capacities of the MOF-Acrylic fabric mixtures were still investigated.

Results for the MOF-Acrylic fabric mixture (AK700) are given below. Surprisingly, this sample showed the highest CO_2 adsorption capacity at 3.97 mmol/g even though immobilization was not achieved as it was intended for the experiment. This is likely due to inclusion of nitrous groups emerged when the acrylic fabric structure was decomposed during the synthesis reaction. Inclusion of nitrous groups improves adsorption capacity (S. Chen et al. 2021) by giving way to chemisorption of CO_2. The experimental adsorption and desorption isotherms for the MOF-Acrylic fabric mixture are given in Figure 31 below.

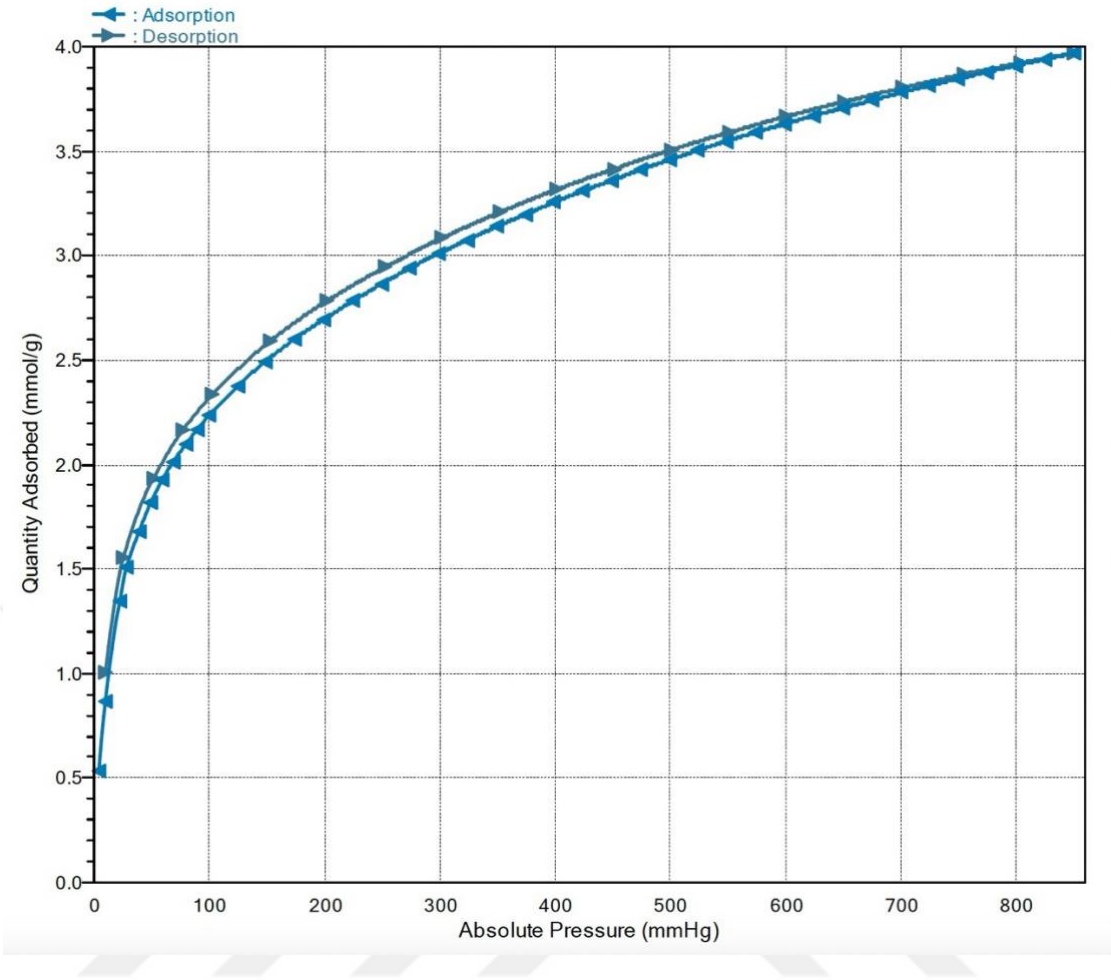

Figure 31. Adsorption and desorption isotherms for MOF-Acrylic fabric decomposed mixture (AK700)

It is observed that both adsorption and desorption isotherms show similar forms to synthesized Ni-MOF-74 powder. Thus, it can be said that MOF-Acrylic fabric mixture also follows a Type I isotherm (IUPAC 1985).

In order to evaluate the adsorption behavior of MOF-Acrylic fabric mixture, experimental adsorption data was fitted to adsorption isotherm models. For this study, Langmuir and Freundlich models were investigated. Figure 32 below demonstrates the fitting to the Langmuir model while Figure 33 demonstrates the fitting to the Freundlich model.

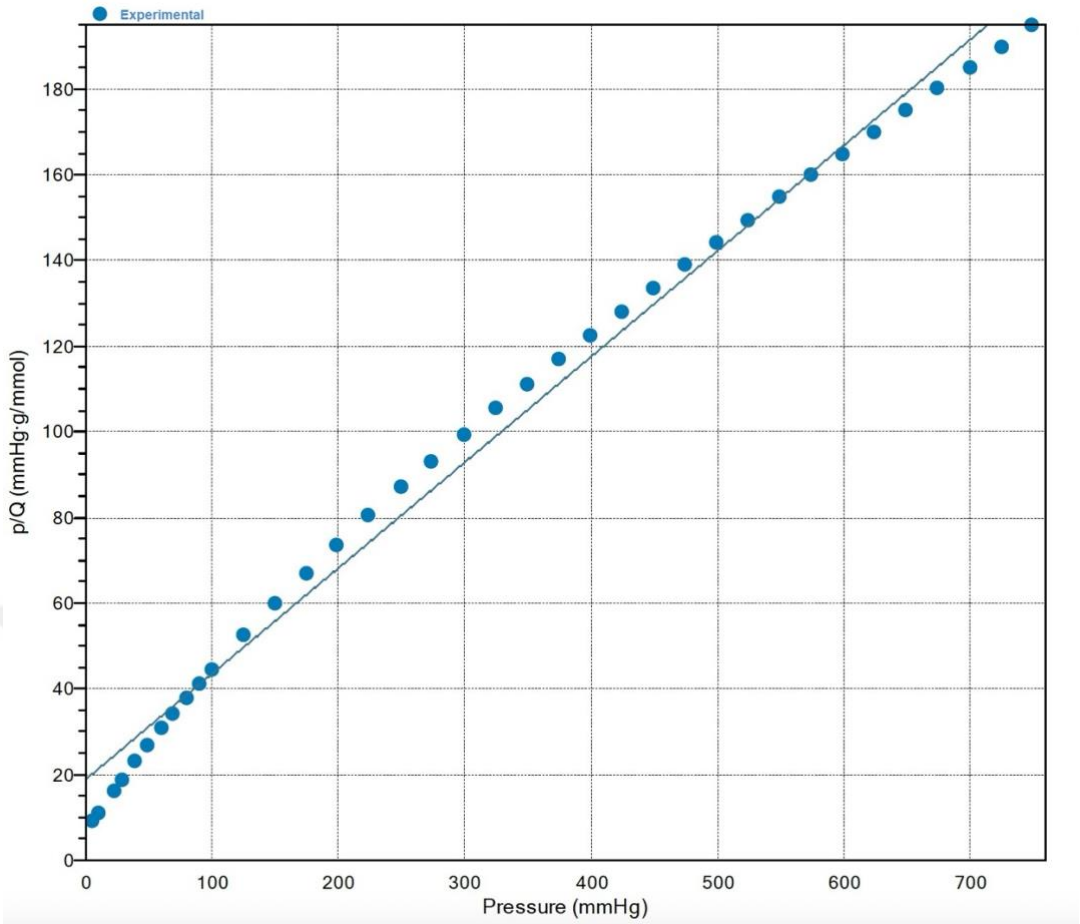

Figure 32. Langmuir adsorption isotherm of MOF-Acrylic fabric decomposed mixture (AK700)

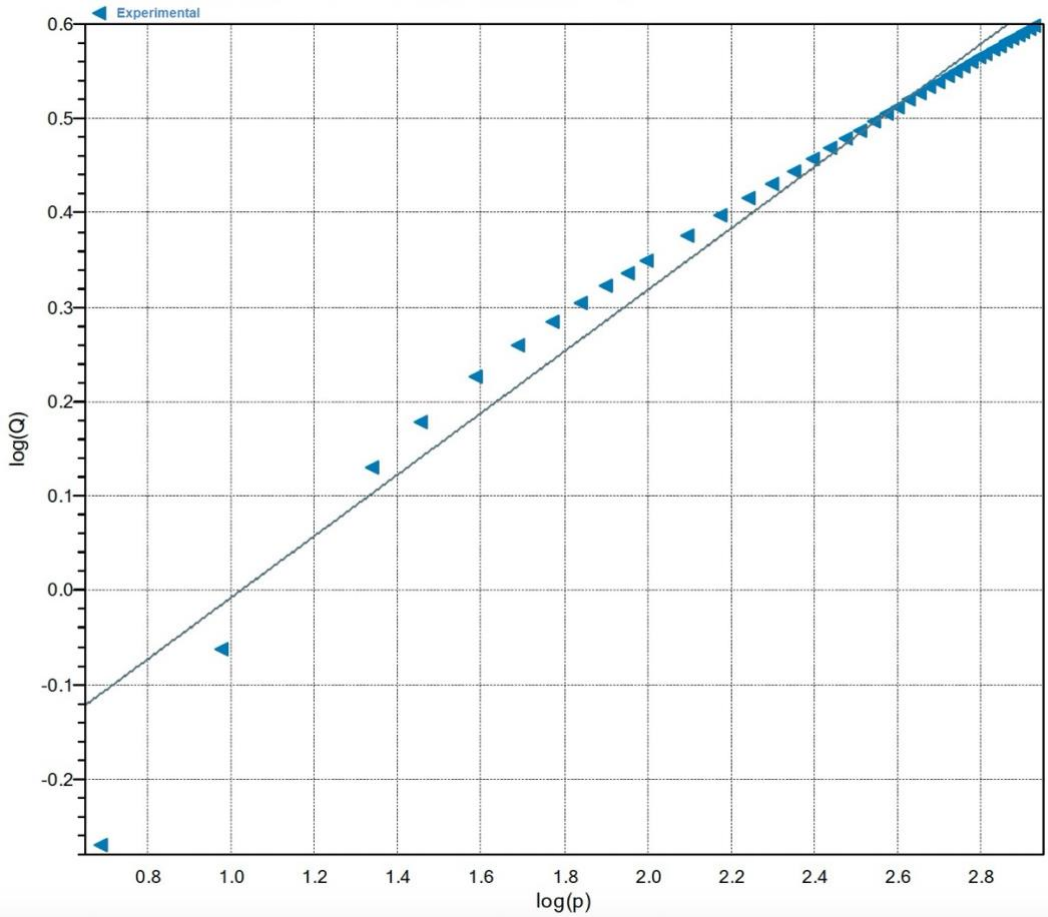

Figure 33. Freundlich adsorption isotherm of MOF-Acrylic fabric decomposed mixture (AK700)

Table 9. CO_2 adsorption isotherm parameters for MOF-Acrylic fabric decomposed mixture (AK700)

Parameters Langmuir isotherm	**Langmuir isotherm**	**Parameters Freundlich**	**Freundlich isotherm**
Temperature(k)	273.15	**Temperature(k)**	273.15
Qm (mmol/g)	4.05472	**Qm.C (mmol/g)**	0.4634
b	0.013079	**n**	3.0665
R	0.9995741	**R**	0.983036

It is quite apparent that the Langmuir model better fit the adsorption behavior of MOF-acrylic fabric mixture based on the correlation coefficient (r^2) of 0.9995741. On the other hand, the Freundlich model shows a correlation coefficient (r^2) of 0.983036. Suitability to Langmuir isotherm suggests monolayer adsorption.

Results for the MOF-Acrylic fabric mixture (ATIII) are also given below. This sample also showed a highest CO_2 adsorption capacity of 3.88 mmol/g even though immobilization was not achieved as it was intended for the experiment. The effect of nitrous groups on the CO_2 adsorption capacity is also observed for this *in-situ* dip coating sample. The experimental adsorption and desorption isotherms for the MOF-Acrylic fabric mixture are given below.

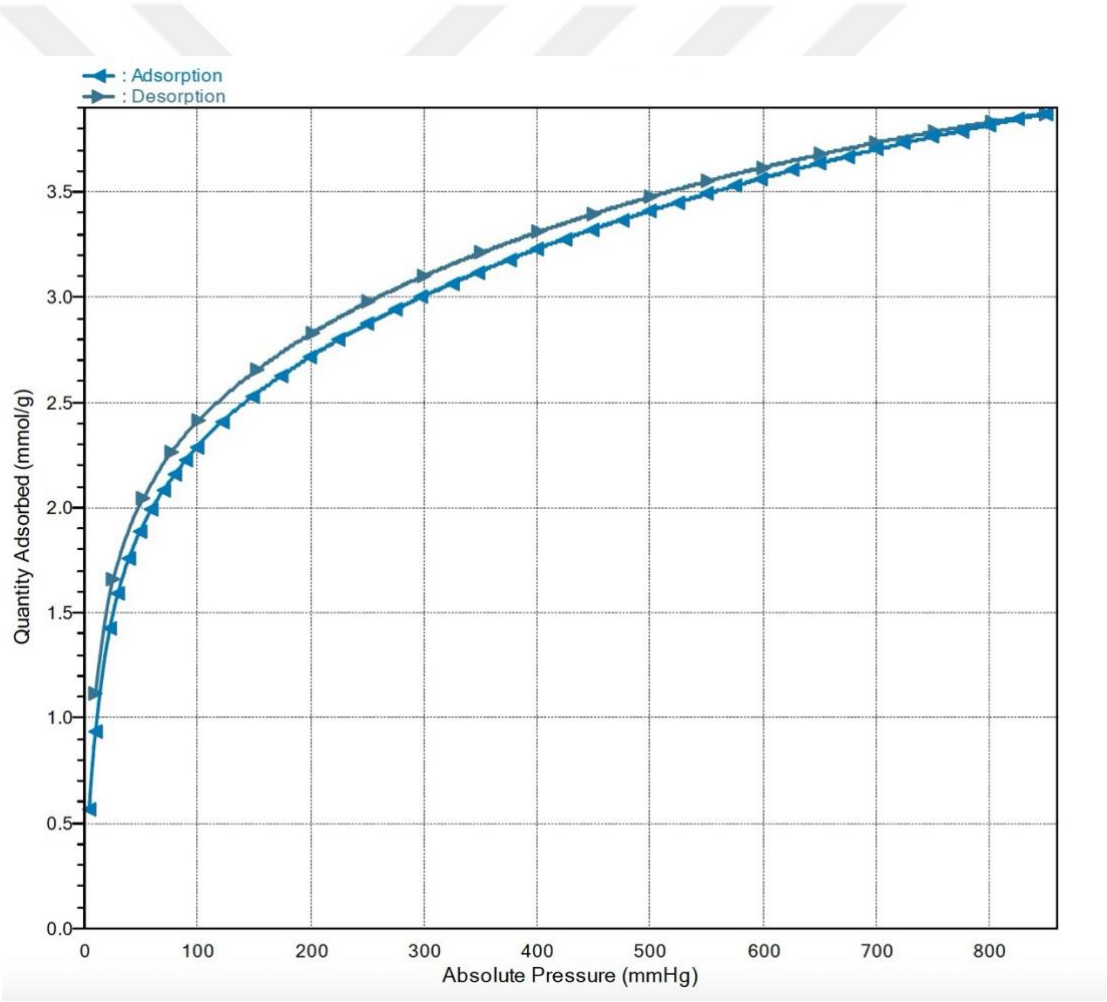

Figure 34. Adsorption and desorption isotherms for MOF-Acrylic fabric decomposed mixture (ATIII)

Similarly, both adsorption and desorption isotherms are compatible to those of synthesized Ni-MOF-74 powder.

In order to evaluate the adsorption behavior of MOF-Acrylic fabric mixture (ATIII), experimental adsorption data was fitted to adsorption isotherm models. For this study, Langmuir and Freundlich models were investigated. Figure 35 below demonstrates the fitting to the Langmuir model while Figure 36 demonstrates the fitting to the Freundlich model. CO_2 adsorption isotherm parameters for the sample were also summarized in Table 10 below.

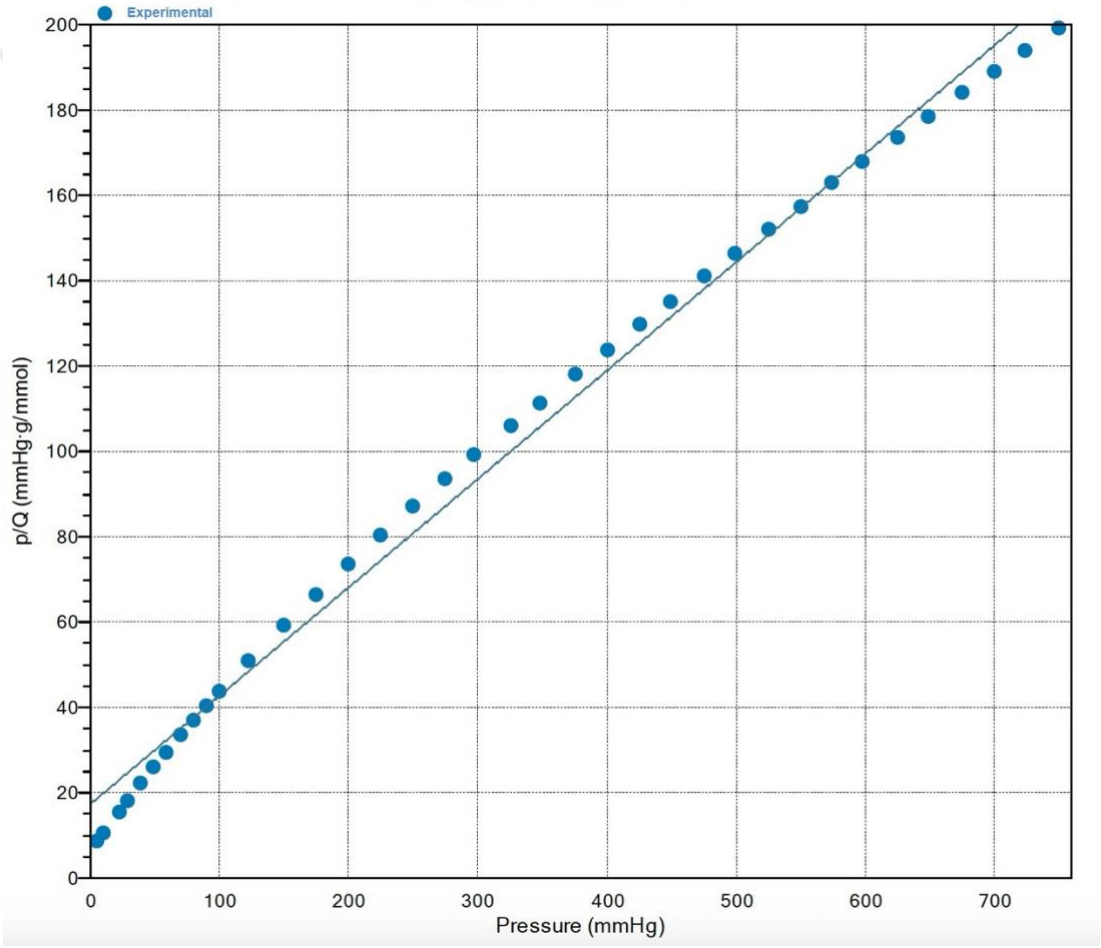

Figure 35. Langmuir adsorption isotherm of MOF-Acrylic fabric decomposed mixture (ATIII)

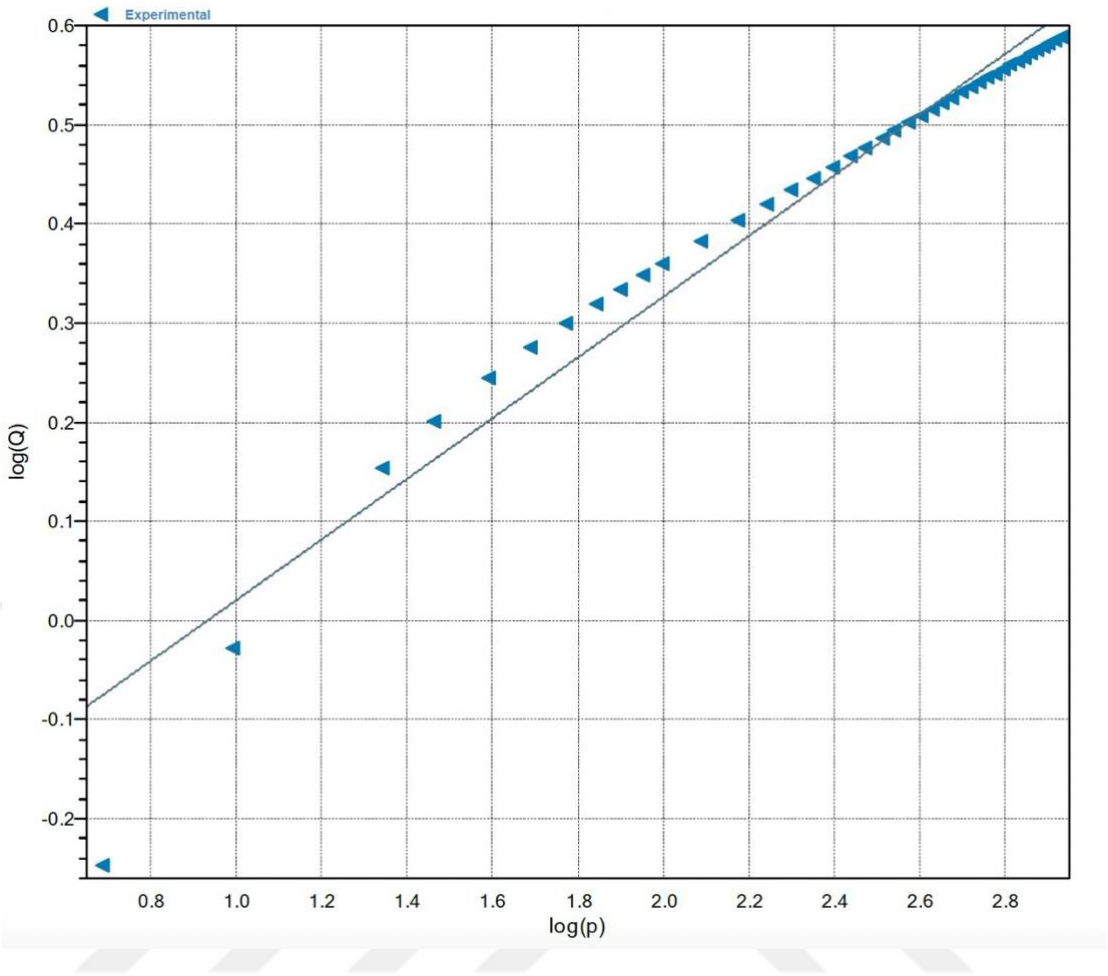

Figure 36. Freundlich adsorption isotherm of MOF-Acrylic fabric decomposed mixture (ATIII)

Table 10. CO_2 adsorption isotherm parameters for MOF-Acrylic fabric decomposed mixture (ATIII)

Parameters Langmuir isotherm	**Langmuir isotherm**	**Parameters Freundlich**	**Freundlich isotherm**
Temperature (K)	273.15	**Temperature (K)**	273.15
Qm (mmol/g)	3.93771	**Qm.C (mmol/g)**	0.5177
b	0.014667	**n**	3.26
R	0.996509	**R**	0.978732

It is observed that Langmuir model better fit the adsorption behavior of MOF-acrylic fabric mixture based on the correlation coefficient (r^2) of 0.996509. On the other hand, the Freundlich model shows a correlation coefficient (r^2) of 0.978732. Suitability to Langmuir isotherm suggests monolayer adsorption.

This revelation shows that even though the particular immobilization technique did not yield expected results, inclusion of amine groups might be worth further exploration in future studies.

CHAPTER 6

CONCLUSION

This study was conducted in two essential segments first of which involved the synthesis and characterization of a nickel-based metal organic framework showing a promising potential for CO_2 adsorption (Ni-MOF-74). The second part of the study was dedicated to the immobilization of Ni-MOF-74 onto acrylonitrile fabrics, a previously unexplored area. CO_2 adsorption analysis for both synthesized Ni-MOF-74 powders and Ni-MOF-74 coated acrylic fabric was also conducted in order to assess the CO_2 adsorption capacities of the resulting material.

For the synthesis of Ni-MOF-74, a metal-to-organic linker ratio of 1:1 (MOF-74(1:1) yielded a higher surface area (180 cm^2/g) and a superior surface structure compared to a ratio of 2:1 (MOF-74(2:1)) which had a surface area of 144 cm^2/g. However, the surface area achieved for both samples fell short of literature-reported surface areas. This is attributed to the inefficient washing of Ni-MOF-74 product after synthesis. Further investigation into optimizing the washing step for Ni-MOF-74 is suggested to be conducted. In terms of CO_2 adsorption capacities, MOF-74(1:1) showed a CO_2 adsorption capacity of 1.98 mmol/g which was higher than that of MOF-74(2:1) (281.28 mmol/g). This result is in line with the lower surface area and a smoother surface structure of MOF-74(2:1). On the other hand, the CO_2 adsorption capacity of both MOF-74(1:1) and MOF-74(2:1) were found to be lower than available literature data. This is attributed to inefficient washing and incomplete activation of Ni-MOF-74 samples. Further investigation into optimizing the washing and activation step for Ni-MOF-74 is suggested to be conducted. These results are a strong indication of the importance of the purification step when it comes to MOF synthesis. It has also been observed that inclusion of amine groups into Ni-MOF-74 structure result in the improvement of CO_2 adsorption capacity. This incidental observation is noted as a potential area of exploration.

This study contributes to the research on creating opportunities for practical application of Ni-MOF-74 by providing a route for immobilization of Ni-MOF-74

powders on acrylonitrile fabric which is a versatile flexible material that can be integrated into various applications. For the immobilization studies, in-situ dip coating and drip casting methods were employed. The in-situ dip coating method was proved to be unsuitable for Ni-MOF-74 immobilization on acrylic fabric due to the harsh synthesis conditions of Ni-MOF-74 and the reaction between the organic solvent (DMF) and acrylic fabric. On the other hand, the drip casting method resulted in the successful immobilization of synthesized Ni-MOF-74 onto acrylic fabric samples. As per the CO_2 adsorption studies on MOF-coated fabrics, the immobilization process resulted in a slight decrease of 0.16 mmol/g (≅8%) in CO_2 adsorption capacity. This finding suggests a significant potential for utilizing Ni-MOF-74 coated acrylic fabrics in practical applications. However, it can also be concluded that the type of acrylic fiber also impacts the CO_2 adsorption capacity of Ni-MOF-74 coated acrylic fabrics.

Further investigation anticipated to follow this work is the optimization studies for synthesis, purification, and activation of Ni-MOF-74 powders, along with the optimization of immobilization and activation process for Ni-MOF-74 coated acrylic fabrics.

REFERENCES

Akpasi, Stephen Okiemute, and Yusuf Makarfi Isa. 2022. “Review of Carbon Capture and Methane Production from Carbon Dioxide.” *Atmosphere*. MDPI. https://doi.org/10.3390/atmos13121958.

Amini, Shima, Homeira Ebrahimzdeh, Shahram Seidi, and Niloofar Jalilian. 2020. “Preparation of Electrospun Polyacrylonitrile/Ni-MOF-74 Nanofibers for Extraction of Atenolol and Captopril Prior to HPLC-DAD.” *Microchimica Acta* 187 (9). https://doi.org/10.1007/s00604-020-04483-5.

Aniruddha, R., I. Sreedhar, and Benjaram M. Reddy. 2020. “MOFs in Carbon Capture-Past, Present and Future.” *Journal of CO2 Utilization*. Elsevier Ltd. https://doi.org/10.1016/j.jcou.2020.101297.

Bastos-Neto, Moises, Diana Cristina Silva de Azevedo, and Sebastião Mardônio Pereira de Lucena. 2020. “Adsorption.” In *Kirk-Othmer Encyclopedia of Chemical Technology*, 1–59. Wiley. https://doi.org/10.1002/0471238961.0104191518212008.a01.pub3.

Calvin, Katherine, Dipak Dasgupta, Gerhard Krinner, Aditi Mukherji, Peter W. Thorne, Christopher Trisos, José Romero, et al. 2023. “IPCC, 2023: Climate Change 2023: Synthesis Report. Contribution of Working Groups I, II and III to the Sixth Assessment Report of the Intergovernmental Panel on Climate Change [Core Writing Team, H. Lee and J. Romero (Eds.)]. IPCC, Geneva, Switzerland.” Edited by Paola Arias, Mercedes Bustamante, Ismail Elgizouli, Gregory Flato, Mark Howden, Carlos Méndez-Vallejo, Joy Jacqueline Pereira, et al. https://doi.org/10.59327/IPCC/AR6-9789291691647.

Chemsoon. n.d. “MOF-74(Ni).” Accessed June 13, 2024. http://m.chemsoon.com/product/882977-00-6.html.

Chen, Changwei, Xiangbo Feng, Qing Zhu, Rui Dong, Rui Yang, Yan Cheng, and Chi He. 2019. "Microwave-Assisted Rapid Synthesis of Well-Shaped MOF-74 (Ni) for CO 2 Efficient Capture." *Inorganic Chemistry* 58 (4): 2717–28. https://doi.org/10.1021/acs.inorgchem.8b03271.

Chen, De Li, Hao Shang, Weidong Zhu, and Rajamani Krishna. 2014. "Transient Breakthroughs of CO2/CH4 and C3H6/C3H8 Mixtures in Fixed Beds Packed with Ni-MOF-74." *Chemical Engineering Science* 117 (September):407–15. https://doi.org/10.1016/j.ces.2014.07.008.

Chen, Shujun, Xuejian Li, Jun Duan, Yue Fu, Zeyuan Wang, Min Zhu, and Na Li. 2021. "Investigation of Highly Efficient Adsorbent Based on Ni-MOF-74 in the Separation of CO2 from Natural Gas." *Chemical Engineering Journal* 419 (September). https://doi.org/10.1016/j.cej.2021.129653.

Cho, Hye-Young, Da-Ae Yang, Jun Kim, Soon-Yong Jeong, and Wha-Seung Ahn. 2012. "CO_2 Adsorption and Catalytic Application of Co-MOF-74 Synthesized by Microwave Heating." *Catalysis Today* 185 (1): 35–40. https://doi.org/https://doi.org/10.1016/j.cattod.2011.08.019.

Choe, Jong Hyeak, Hyojin Kim, and Chang Seop Hong. 2021. "MOF-74 Type Variants for CO_2 capture." *Materials Chemistry Frontiers*. Royal Society of Chemistry. https://doi.org/10.1039/d1qm00205h.

Choi, Chungjung, Rahul L. Kadam, Sanjit Gaikwad, Kyu Suk Hwang, and Sangil Han. 2020. "Metal Organic Frameworks Immobilized Polyacrylonitrile Fiber Mats with Polyethyleneimine Impregnation for CO2 Capture." *Microporous and Mesoporous Materials* 296 (April). https://doi.org/10.1016/j.micromeso.2020.110006.

Ding, Meili, Robinson W. Flaig, Hai Long Jiang, and Omar M. Yaghi. 2019. "Carbon Capture and Conversion Using Metal-Organic Frameworks and MOF-Based Materials." *Chemical Society Reviews*. Royal Society of Chemistry. https://doi.org/10.1039/c8cs00829a.

Douglas M. Ruthven. 1984. *Principles of Adsorption and Adsorption Processes-Wiley-Interscience*. John Wiley & Sons, Ltd.

Energy Agency, International. n.d. "The Role of CCUS in Low-Carbon Power Systems."

Fajrina, N., N. Yusof, A. F. Ismail, J. Jaafar, F. Aziz, and W. N.W. Salleh. 2022. "Metal Organic Framework (MOF)-Based Composite Filler Incorporated Thin Film Nanocomposite of Hollow Fiber Membrane for Carbon Dioxide Permeance." *Materials Today: Proceedings* 65 (January):3060–65. https://doi.org/10.1016/j.matpr.2022.04.125.

Ghanbari, Taravat, Faisal Abnisa, and Wan Mohd Ashri Wan Daud. 2020. "A Review on Production of Metal Organic Frameworks (MOF) for CO_2 Adsorption." *Science of the Total Environment*. Elsevier B.V. https://doi.org/10.1016/j.scitotenv.2019.135090.

Goel, Priyanshu, Shalini Singh, Harmeet Kaur, Sunita Mishra, and Akash Deep. 2021. "Low-Cost Inkjet Printing of Metal–Organic Frameworks Patterns on Different Substrates and Their Applications in Ammonia Sensing." *Sensors and Actuators, B: Chemical* 329 (February). https://doi.org/10.1016/j.snb.2020.129157.

Grant Glover, T., Gregory W. Peterson, Bryan J. Schindler, David Britt, and Omar Yaghi. 2011. "MOF-74 Building Unit Has a Direct Impact on Toxic Gas Adsorption." *Chemical Engineering Science* 66 (2): 163–70. https://doi.org/10.1016/j.ces.2010.10.002.

Greig, Chris, and Sam Uden. 2021. "The Value of CCUS in Transitions to Net-Zero Emissions." *Electricity Journal* 34 (7). https://doi.org/10.1016/j.tej.2021.107004.

Haque, Enamul, and Sung Hwa Jhung. 2011. "Synthesis of Isostructural Metal-Organic Frameworks, CPO-27s, with Ultrasound, Microwave, and Conventional Heating: Effect of Synthesis Methods and Metal Ions." *Chemical Engineering Journal* 173 (3): 866–72. https://doi.org/10.1016/j.cej.2011.08.037.

Harandizadeh, Amir Hossein, Seyedfoad Aghamiri, Mohammad Hojjat, Marziyeh Ranjbar-Mohammadi, and Mohammad Reza Talaie. 2022. "Adsorption of Carbon Dioxide with Ni-MOF-74 and MWCNT Incorporated Poly Acrylonitrile Nanofibers." *Nanomaterials* 12 (3). https://doi.org/10.3390/nano12030412.

Hu, Zhigang, Yuxiang Wang, Bhuvan B. Shah, and Dan Zhao. 2019. "CO_2 Capture in Metal–Organic Framework Adsorbents: An Engineering Perspective." *Advanced Sustainable Systems* 3 (1). https://doi.org/10.1002/adsu.201800080.

IUPAC. 1985. "International Union Of Pure And Applied Chemistry Physical Chemistry Division Commission On Colloid And Surface Chemistry Including Catalysis Reporting Physisorption Data For Gas/Solid Systems with Special Reference to the Determination of Surface Area and Porosity Reporting Physisorption Data for Gas/Solid Systems-with Special Reference to the Determination of Surface Area and Porosity."

Jodłowski, P. J., G. Kurowski, K. Dymek, R. J. Jędrzejczyk, P. Jeleń, Kuterasiński, A. Gancarczyk, A. Węgrzynowicz, T. Sawoszczuk, and M. Sitarz. 2020. "In Situ Deposition of M(M=Zn; Ni; Co)-MOF-74 over Structured Carriers for Cyclohexene Oxidation - Spectroscopic and Microscopic Characterisation." *Microporous and Mesoporous Materials* 303 (August). https://doi.org/10.1016/j.micromeso.2020.110249.

Jürgen U. Keller, and Reiner Staudt. 2005. *Gas Adsorption Equilibria Experimental Methods and Adsorptive Isotherms*. Springer Science + Business Media, Inc.

Kalmutzki, Markus J, Nikita Hanikel, and Omar M Yaghi. 2018. "Secondary Building Units as the Turning Point in the Development of the Reticular Chemistry of MOFs." *Sci. Adv.* Vol. 4. https://www.science.org.

Kamal, Khaliesah, Mohamad Azmi Bustam, Marhaina Ismail, Denys Grekov, Azmi Mohd Shariff, and Pascaline Pré. 2020. "Optimization of Washing Processes in Solvothermal Synthesis of Nickel-Based Mof-74." *Materials* 13 (12): 1–10. https://doi.org/10.3390/ma13122741.

Keskin, Seda, Timothy M. van Heest, and David S. Sholl. 2010a. “Can Metal-Organic Framework Materials Play a Useful Role in Large-Scale Carbon Dioxide Separations?” *ChemSusChem* 3 (8): 879–91. https://doi.org/10.1002/cssc.201000114.

Keskin, Seda, Timothy M. van Heest, and David S. Sholl. 2010b. “Can Metal-Organic Framework Materials Play a Useful Role in Large-Scale Carbon Dioxide Separations?” *ChemSusChem*. Wiley-VCH Verlag. https://doi.org/10.1002/cssc.201000114.

Kitagawa, Susumu, and Ryotaro Matsuda. 2007. “Chemistry of Coordination Space of Porous Coordination Polymers.” *Coordination Chemistry Reviews*. https://doi.org/10.1016/j.ccr.2007.07.009.

Kuppler, Ryan J., Daren J. Timmons, Qian Rong Fang, Jian Rong Li, Trevor A. Makal, Mark D. Young, Daqiang Yuan, Dan Zhao, Wenjuan Zhuang, and Hong Cai Zhou. 2009. “Potential Applications of Metal-Organic Frameworks.” *Coordination Chemistry Reviews*. https://doi.org/10.1016/j.ccr.2009.05.019.

Lesmana, Sisca O, Novie Febriana, Felycia E Soetaredjo, Jaka Sunarso, and Suryadi Ismadji. 2009. “Studies on Potential Applications of Biomass for the Separation of Heavy Metals from Water and Wastewater.” *Biochemical Engineering Journal* 44 (1): 19–41. https://doi.org/https://doi.org/10.1016/j.bej.2008.12.009.

Leung, Dennis Y.C., Giorgio Caramanna, and M. Mercedes Maroto-Valer. 2014. “An Overview of Current Status of Carbon Dioxide Capture and Storage Technologies.” *Renewable and Sustainable Energy Reviews*. Elsevier Ltd. https://doi.org/10.1016/j.rser.2014.07.093.

Li, Zong-Qun, Ling-Guang Qiu, Tao Xu, Yun Wu, Wei Wang, Zhen-Yu Wu, and Xia Jiang. 2009. “Ultrasonic Synthesis of the Microporous Metal–Organic Framework $Cu_3(BTC)_2$ at Ambient Temperature and Pressure: An Efficient and Environmentally Friendly Method.” *Materials Letters* 63 (1): 78–80. https://doi.org/https://doi.org/10.1016/j.matlet.2008.09.010.

Liang, Weibin, Prashant M. Bhatt, Aleksander Shkurenko, Karim Adil, Georges Mouchaham, Himanshu Aggarwal, Arijit Mallick, Aqil Jamal, Youssef Belmabkhout, and Mohamed Eddaoudi. 2019. "A Tailor-Made Interpenetrated MOF with Exceptional Carbon-Capture Performance from Flue Gas." *Chem* 5 (4): 950–63. https://doi.org/10.1016/j.chempr.2019.02.007.

Lin, Xiaoying, Weipeng Zeng, Minyi Liu, Qinhua Zhong, Ting Su, Linzhu Gong, and Yamin Liu. 2023. "Amino-Modified Mg-MOF-74: Synthesis, Characterization and CO2 Adsorption Performance." *Environmental Engineering Research* 28 (1). https://doi.org/10.4491/eer.2021.569.

Liu, Jian, Annabelle I. Benin, Amanda M.B. Furtado, Paulina Jakubczak, Richard R. Willis, and M. Douglas Levan. 2011. "Stability Effects on CO2 Adsorption for the DOBDC Series of Metal-Organic Frameworks." *Langmuir* 27 (18): 11451–56. https://doi.org/10.1021/la201774x.

Ma, Kaikai, Karam B. Idrees, Florencia A. Son, Rodrigo Maldonado, Megan C. Wasson, Xuan Zhang, Xingjie Wang, et al. 2020. "Fiber Composites of Metal-Organic Frameworks." *Chemistry of Materials*. American Chemical Society. https://doi.org/10.1021/acs.chemmater.0c02379.

Martinez-Diaz, David, Pedro Leo, David Martín Crespo, María Sánchez, and Alejandro Ureña. 2024. "Direct Synthesis of MOF-74 Materials on Carbon Fiber Electrodes for Structural Supercapacitors." *Nanomaterials* 14 (2). https://doi.org/10.3390/nano14020227.

Millward, Andrew R., and Omar M. Yaghi. 2005. "Metal-Organic Frameworks with Exceptionally High Capacity for Storage of Carbon Dioxide at Room Temperature." *Journal of the American Chemical Society* 127 (51): 17998–99. https://doi.org/10.1021/ja0570032.

Nakao Shin-ichi and Yogo, Katsunori and Goto Kazuya and Kai Teruhiko and Yamada Hidetaka. 2019. "Introduction." In *Advanced CO2 Capture Technologies:*

Absorption, Adsorption, and Membrane Separation Methods, 1–2. Cham: Springer International Publishing. https://doi.org/10.1007/978-3-030-18858-0_1.

Nandi, Shyamapada, Himan Dev Singh, Debanjan Chakraborty, Rahul Maity, and Ramanathan Vaidhyanathan. 2021. "Deciphering the Weak CO_2 Framework Interactions in Microporous MOFs Functionalized with Strong Adsorption Sites—A Ubiquitous Observation." *ACS Applied Materials & Interfaces* 13 (21): 24976–83. https://doi.org/10.1021/acsami.1c05845.

Olabi, A. G., Tabbi Wilberforce, Khaled Elsaid, Enas Taha Sayed, Hussein M. Maghrabie, and Mohammad Ali Abdelkareem. 2022. "Large Scale Application of Carbon Capture to Process Industries – A Review." *Journal of Cleaner Production*. Elsevier Ltd. https://doi.org/10.1016/j.jclepro.2022.132300.

Pettinari, Claudio, and Alessia Tombesi. 2020. "Metal–Organic Frameworks for Carbon Dioxide Capture." *MRS Energy and Sustainability*. Springer Nature. https://doi.org/10.1557/mre.2020.30.

Rezaei, Fateme, Shane Lawson, Hooman Hosseini, Harshul Thakkar, Amit Hajari, Saman Monjezi, and Ali A. Rownaghi. 2017a. "MOF-74 and UTSA-16 Film Growth on Monolithic Structures and Their CO2 Adsorption Performance." *Chemical Engineering Journal* 313:1346–53. https://doi.org/10.1016/j.cej.2016.11.058.

Rezaei, Fateme, Shane Lawson, Hooman Hosseini, Harshul Thakkar, Amit Hajari, Saman Monjezi, and Ali A. Rownaghi. 2017b. "MOF-74 and UTSA-16 Film Growth on Monolithic Structures and Their CO2 Adsorption Performance." *Chemical Engineering Journal* 313:1346–53. https://doi.org/10.1016/j.cej.2016.11.058.

Rowsell, Jesse L.C., and Omar M. Yaghi. 2004. "Metal-Organic Frameworks: A New Class of Porous Materials." *Microporous and Mesoporous Materials*. https://doi.org/10.1016/j.micromeso.2004.03.034.

Ruthven, Douglas M. 2001. “Adsorption, Fundamentals.” In *Kirk-Othmer Encyclopedia of Chemical Technology*. John Wiley & Sons, Ltd. https://doi.org/10.1002/0471238961.0104191518212008.a01.pub2.

Safaei, Mohadeseh, Mohammad Mehdi Foroughi, Nasser Ebrahimpoor, Shohreh Jahani, Ali Omidi, and Mehrdad Khatami. 2019. “A Review on Metal-Organic Frameworks: Synthesis and Applications.” *TrAC - Trends in Analytical Chemistry*. Elsevier B.V. https://doi.org/10.1016/j.trac.2019.06.007.

Sifat, Najmus S., and Yousef Haseli. 2019. “A Critical Review of CO2 Capture Technologies and Prospects for Clean Power Generation.” *Energies*. MDPI AG. https://doi.org/10.3390/en12214143.

Sreenivasulu, B., D. V. Gayatri, I. Sreedhar, and K. V. Raghavan. 2015. “A Journey into the Process and Engineering Aspects of Carbon Capture Technologies.” *Renewable and Sustainable Energy Reviews*. Elsevier Ltd. https://doi.org/10.1016/j.rser.2014.09.029.

Stuart, Barbara H. 2004. *Infrared Spectroscopy: Fundamentals and Applications*. John Wiley & Sons, Ltd.

Teo, Wei Liang, Jiawei Liu, Weiqiang Zhou, and Yanli Zhao. 2021. “Facile Preparation of Antibacterial MOF-Fabric Systems for Functional Protective Wearables.” *SmartMat* 2 (4): 567–78. https://doi.org/10.1002/smm2.1046.

UNEP. 2023. “UNEP Emissions Gap Report 2023.” https://doi.org/10.59117/20.500.11822/43922.

Wang, Qian, Junfeng Bai, Zhiyong Lu, Yi Pan, and Xiaozeng You. 2016. “Finely Tuning MOFs towards High-Performance Post-Combustion CO2 Capture Materials.” *Chemical Communications* 52 (3): 443–52. https://doi.org/10.1039/c5cc07751f.

Wang, Xiaoxing, and Chunshan Song. 2020. “Carbon Capture From Flue Gas and the Atmosphere: A Perspective.” *Frontiers in Energy Research*. Frontiers Media S.A. https://doi.org/10.3389/fenrg.2020.560849.

Wilberforce, Tabbi, A. G. Olabi, Enas Taha Sayed, Khaled Elsaid, and Mohammad Ali Abdelkareem. 2021. “Progress in Carbon Capture Technologies.” *Science of the Total Environment* 761 (March). https://doi.org/10.1016/j.scitotenv.2020.143203.

Wu, Xiaofei, Zongbi Bao, Bin Yuan, Jun Wang, Yingqiang Sun, Hongmei Luo, and Shuguang Deng. 2013. “Microwave Synthesis and Characterization of MOF-74 (M = Ni, Mg) for Gas Separation.” *Microporous and Mesoporous Materials* 180:114–22. https://doi.org/10.1016/j.micromeso.2013.06.023.

Yangyang Liu, Zhiyong U. Wang, and Hong-Cai Zhou. 2012. “Recent Advances in Carbon Dioxide with Metal-Organic.” *Greenhouse Gases: Science and Technology* 2 (5): 352–68. https://doi.org/https://doi.org/10.1002/ghg.1296.

Yazaydin, A. Özgür, Randall Q. Snurr, Tae Hong Park, Kyoungmoo Koh, Jian Liu, M. Douglas LeVan, Annabelle I. Benin, et al. 2009. “Screening of Metal-Organic Frameworks for Carbon Dioxide Capture from Flue Gas Using a Combined Experimental and Modeling Approach.” *Journal of the American Chemical Society* 131 (51): 18198–99. https://doi.org/10.1021/ja9057234.

Yazaydın, A Özgür, Annabelle I Benin, Syed A Faheem, Paulina Jakubczak, John J Low, Richard R Willis, and Randall Q Snurr. 2009. “Enhanced CO2 Adsorption in Metal-Organic Frameworks via Occupation of Open-Metal Sites by Coordinated Water Molecules.” *Chemistry of Materials* 21 (8): 1425–30. https://doi.org/10.1021/cm900049x.

Yu, Mei Hui, Lin Geng, Ze Chang, and Xian He Bu. 2023. “Coordination Bonding Directed Molecular Assembly toward Functional Metal-Organic Frameworks: From Structural Regulation to Properties Modulation.” *Accounts of Materials Research* 4 (10): 839–53. https://doi.org/10.1021/accountsmr.3c00097.